




On the sliding frictional nanocontact of an exponentially graded layer/substrate structure

Rui Cao · Jie Yan · Changwen Mi 

Received: 1 July 2022 / Accepted: 30 October 2022 / Published online: 21 November 2022
© The Author(s), under exclusive licence to Springer Nature B.V. 2022

Abstract This paper analyzes the sliding frictional nanocontact of an exponentially graded layer perfectly bonded to a homogeneous half-plane substrate under the nanoindentation of a rigid cylinder. The punch is subjected to both normal and tangential loads, satisfying Coulomb's friction law. The contact interface is modeled by the full version of Steigmann–Ogden surface mechanical theory, in which surface tension, surface membrane stiffness and surface flexural rigidity are all taken into account. The method of Fourier integral transforms was applied to convert the governing equations and nonclassical boundary conditions into a Fredholm integral equation. By separating a nonsingular term from the integrand of the kernel function of the integral equation, numerical integration of the kernel function can be significantly improved. After that, Gauss–Chebyshev numerical quadratures are further employed to discretize and collocate the integral equation and the indentation force equilibrium condition. An iterative algorithm is subsequently developed to solve the resultant nonlinear algebraic system regarding

discretized contact pressures and the two asymmetric contact boundaries. Stresses and displacements in the layer/substrate structure are also determined for completeness. Extensive parametric studies clarify the relative importance among three surface parameters, all helping to partially carry on the indentation loading in addition to the conventional bulk portion of the layer/substrate system. The sliding frictional condition significantly affects the symmetry of the contact pressure distribution and contact zone. The property gradation of the layer is another important factor affecting contact properties. The results reported in the current work show a concrete means of tailoring nanocontact responses of graded layers in nanosized materials and devices.

Keywords Nanocontact · Graded layer · Sliding friction · Surface flexural rigidity · Surface tension · Rigid cylinder

1 Introduction

Graded materials are a class of composites that contain two or more constituent phases. The mechanical properties of a graded material may vary continuously along one or more dimensions, in order to achieve desired functionalities. Graded materials have found their applications in metals, ceramics and organic composites, for the purpose of improving the thermal, wear and corrosion prevention capabilities

R. Cao · C. Mi (✉)
Jiangsu Key Laboratory of Engineering Mechanics,
School of Civil Engineering, Southeast University,
Nanjing 210096, Jiangsu, China
e-mail: mi@seu.edu.cn

J. Yan
Department of Road Traffic Management, Sichuan Police
College, Luzhou 646000, Sichuan, China

(Schulz et al. 2003; Zhou et al. 2021; Argatov and Chai 2022). Suresh (2001) reported that, with a suitable spatial variation of elastic modulus, a graded layer can provide effective resistance to deformations and damages under the condition of spherical or conical indentations.

Benefitting from their continuous gradation of mechanical properties, numerous studies have been conducted to study the contact properties of graded materials. We start the literature review from the frictional contact of graded half-planes and half-spaces. Elloumi et al. (2010) explored the partial slip contact of a graded half-plane under the indentation of a rigid stamp. Dag et al. (2013) investigated the sliding frictional contact of a laterally graded substrate indented by a rigid punch with an arbitrary profile. Both semi-analytical and finite element solutions were provided for the contact pressure and contact boundaries. For a graded orthotropic half-plane, Kucuksucu et al. (2015) and Guler et al. (2017) solved the frictional contact problem under the indentation of a rigid flat-ended and cylindrical punch, respectively. Chen et al. (2015) further analyzed the contact problem between a rigid roller and a graded half-plane with an arbitrary gradient direction. In addition to single-direction gradation, Arslan (2020) examined the sliding frictional contact of a bidirectionally graded half-plane.

The above literature papers treat the whole half-plane or half-space as a graded medium. Engineering practice prefers to applying graded materials as a layer or a transitional medium. Guler and Erdogan (2007) investigated the sliding frictional contact of a graded layer bonded to a homogeneous half-plane. The effects of layer property gradation, frictional coefficient and geometry were analyzed in detail. Yang and Ke (2008) studied the contact properties of a graded transitional layer that is sandwiched between a homogeneous layer and a homogeneous substrate. The contact pressure and contact size were solved for the case of a rigid cylinder. Taking the frictional heat into account, Choi and Paulino (2008) reanalyzed the same contact problem by the use of the steady-state plane thermoelasticity theory. Jobin et al. (2017) developed a semianalytical solution for an inhomogeneously coated half-plane under the indentation of rigid stamps. The graded layer was discretized into multiple homogeneous sublayers. Such a multilayered discretization strategy works particularly well for graded layers with an arbitrary property gradation.

Attia and El-Shafei (2019) developed finite element solutions to the nonlinear contact problem of graded layered materials. Arslan and Dag (2018) investigated the sliding frictional contact of an orthotropic layer/substrate structure. The dynamic frictional contact problems of a graded layer subjected to a moving cylinder (Balci and Dag 2019) or an angular-ended indenter (Balci and Dag 2020) have also been solved. In addition to the sliding frictional condition, the rolling contact between a graded layer and a rolling cylinder under the simultaneous applications of normal and tangential forces has also been considered (Alinia et al. 2014).

The frictional contact problems reviewed above were all studied with the classical theory of elasticity. The solutions are valid for regular scale contact models. However, as the indenter size in those contact models approaches to microscale, the contact zone will fall into the nanoscale. Under such a small length scale, surface effects enter into the mechanics and physics of contact problems. Numerous theoretical and experimental results have shown that surface effects have an evident impact on the mechanical properties of nanosized materials and structures (Cammarata 1994; Zhang et al. 2008; Rahman et al. 2016; Wang 2019). The very high surface-to-volume ratio in these materials and structures is responsible for surface effects. Gurtin and Murdoch (1975, 1978) proposed the first surface mechanical theory for solid materials. In this theory, a solid surface is treated as an elastic membrane possessing zero thickness and perfectly bonded to its abutting bulk solid. In addition to surface tension, the resistibility of a solid surface to in-plane stretching and shear deformations is also accommodated. For this reason, Gurtin–Murdoch surface mechanical theory is able to reflect the size-dependent feature of nanoscale materials and structures to a certain extent (Shenoy 2002; Mi et al. 2008).

In contact mechanics, Gurtin–Murdoch surface theory and its variants were first employed to analyze the nanocontact properties of homogeneous layers, half-planes and half-spaces subjected to traction loads. Zhao and Rajapakse (2009) determined the displacements and stresses in a two-dimensional homogeneous elastic layer bonded to a rigid substrate under the application of localized normal and tangential traction forces. Zhao and Rajapakse (2013) further considered a three-dimensional homogeneous

layer subjected to localized tangential traction loads. The asymmetric displacements and stresses were determined. Zhou and Gao (2013) developed analytical solutions for homogeneous half-planes and half-spaces subjected to a distributive normal pressure. Mi (2017) investigated the asymmetric problem of a homogeneous half-space under the application of localized tangential tractions. Different from the conventional isotropic assumption, Shen (2019) restudied Boussinesq problem for a transversely isotropic half-space incorporating surface effects. Moradweysi et al. (2019) solved the contact problem of a homogeneous half-space by the coupling of strain gradient and surface theories. Le et al. (2021) analyzed the elastic response of a homogeneous half-plane under the application of normal, shear and couple tractions. The coupling effects of couple stress and Gurtin–Murdoch surface elasticity were studied.

The nanocontact properties of elastic layers, half-planes and half-spaces under the indentation of rigid stamps have also been studied with the account of surface effects. Due to the additional complexity introduced by mixed boundary conditions, this line of research is primarily concerned with frictionless contact problems. Argatov and Sabina (2012) addressed the spherical indentation of a transversely isotropic half-space reinforced by an extensible membrane. Pinyochotiwong et al. (2013) solved the nanocontact problem between an elastic half-space and a rigid indenter. Besides the conventional semianalytical approach, Gad et al. (2014) developed a finite element formulation to numerically analyze the nanocontact properties of a two-dimensional elastic strip. Tirapat et al. (2020) solved the nanoscale adhesive contact problem of a homogeneous elastic layer possessing a Gurtin–Murdoch type boundary that is indented by a flat-ended cylinder. Assuming an inner adhesion zone and an outer finite friction zone, Intarit et al. (2020) reconsidered the nanocontact model.

The nanocontact problems reviewed above neglected the resistibility of a solid surface to flexural deformations, since the solid surface is modeled as an elastic membrane without any bending rigidities (Ban and Mi 2021). By the use of molecular dynamics simulations, Chhapadia et al. (2011) clarified the bending deformation of the lateral surfaces of a cantilevered nanowire. They quantitatively evaluated its surface thickness. Their results explained the appreciably larger elastic modulus of a nanowire under

bending than under extension. In fact, longer than two decades ago, Steigmann and Ogden (1997, 1999) have extended the Gurtin–Murdoch surface theory, in order to additionally take the surface bending rigidity into consideration. However, until the recent five years, the improved Steigmann–Ogden surface mechanical has received sufficient attentions (Walton and Zemlyanova 2016; Zemlyanova and Mogilevs-kaya 2018; Zemlyanova 2018, 2019; Mi 2018; Li and Mi 2019a, b, 2021).

As to the nanocontact mechanics of graded materials, much fewer works can be found in the open literature. Attia and Mahmoud (2015) proposed a finite element scheme for the frictionless nanoindentation of an elastic substrate reinforced with a power-law graded layer due to rigid or deformable indenters. The complete version of Gurtin–Murdoch surface theory was employed to address the surface effects. Vasu and Bhandakkar (2018) solved the nanocontact problem of an exponentially graded half-plane, reinforced with a Gurtin–Murdoch type boundary. Zhang et al. (2018) explored the frictionless nanocontact responses of a graded layer, by using the surface model proposed by Chen and Yao (2014). Zhu et al. (2019) considered a linearly graded half-plane subjected to uniform surface tractions. Surface tension was incorporated, in order to account for the graded half-plane boundary effects. Ban and Mi (2022) analyzed the competing mechanism between adhesive and surface effects on the determination of the nanocontact behavior of a graded layer/substrate structure.

This work aims at exploring the sliding frictional nanocontact properties of an exponentially graded layer/substrate structure. The exponential variation of the graded coating's shear modulus is not just a mathematical assumption. Existing technology can already synthesize such graded coatings for structural components in order to guard against contact deformation and damage (Giannakopoulos and Suresh 1997). The major originality lies in two aspects. First, the full Steigmann–Ogden surface theory including surface tension, membrane stiffness and flexural rigidity is accounted for. Second, the effects of sliding friction are first considered in the nanocontact mechanics of graded materials. The proposed two-dimensional nanocontact model may be viewed as a plane-strain approximation to the sliding nanoindentation between a rigid microsized cylinder and a three-dimensional coating-substrate structure. The model may also be used as the plane-stress

approximation for the engagement between two micro-sized gears. The remainder of this paper is structured as follows. Section 2 presents the theoretical formulation of the proposed nanocontact problem, leading to a governing Fredholm integral equation. In Sect. 3, the convergence of the infinite integrals inherent to the Fredholm integral equation is analyzed in detail. Along with the indentation force equilibrium equation, a numerical solution algorithm to the governing integral equation is outlined in Sect. 4. Section 5 first validates our method and algorithm against available literature data, followed by extensive parametric studies about surface parameters, frictional coefficient and layer property gradation. Finally, in Sect. 6, a few major conclusions of this work are drawn.

2 Formulation of dual integral equations

2.1 Problem statement

We consider the sliding frictional contact between a rigid cylinder and an exponentially graded layer perfectly bonded to a homogeneous half-plane, as shown in Fig. 1. The graded layer has the finite thickness of h . The rigid cylinder has the radius R and is under the application of both normal (P) and tangential (Q) forces. They satisfy Coulomb's law of friction, i.e., $Q = \eta P$. As a result, the sliding frictional condition is assumed in this work. Due to the presence of friction, the left ($x = -a$) and the right ($x = b$) contact boundaries are not symmetric about the symmetry axis (z) of the rigid cylinder. This is in contrast with frictionless contact.

The shear modulus of the graded layer is assumed to vary as an exponential function of the thickness coordinate

$$\mu(z) = \mu_1 e^{\beta z}, \quad 0 \leq z \leq h, \quad (1)$$

where β is a parameter that characterizes the property gradation along the layer thickness and μ_1 represents the shear modulus of the graded layer at its upper surface ($z = 0$). Since the half-plane substrate is homogeneous, its shear modulus is taken as the constant μ_2 . For simplicity, Poisson's ratios of the layer and the substrate are taken as equal, denoted by Kolosov's constant κ in the subsequent formulation and solution procedure. Under plane strain condition, $\kappa = 3 - 4\nu$.

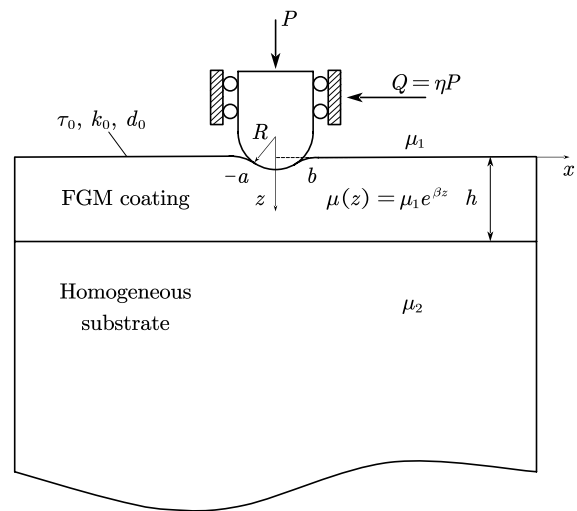


Fig. 1 Geometry and loading configuration of the sliding frictional nanoindentation between a rigid cylinder and an exponentially graded layer perfectly bonded to a homogeneous half-plane substrate

Across the layer/substrate interface, the shear modulus is treated as continuous

$$\mu_2 = \mu_1 e^{\beta h}. \quad (2)$$

The gradient index of the layer can therefore be given by

$$\beta h = \ln \Gamma, \quad (3)$$

where $\Gamma = \mu_2/\mu_1$ denotes the shear moduli ratio between the substrate and the upper surface of the graded layer. Given the geometric model and loading conditions of the nanocontact problem, the fundamental unknowns are identified as the contact pressure and both contact boundaries. Only after they are determined, the elastic fields in the graded layer and the half-plane may be further evaluated.

2.2 Dual integral equations

Under nanoindentation, the contact interface is modeled by the Steigmann–Ogden surface theory (Steigmann and Ogden 1997, 1999; Zemlyanova and Mogilevskaya 2018). Different material properties than those of the abutting layer bulk need to be allocated. They are composed of the surface tension (τ_0), membrane (tensile) stiffness (k_0) and flexural

rigidity (d_0). Steigmann–Ogden surface theory treats a solid surface or interface as a thin plate, possessing surface tension, membrane stiffness and flexural rigidity. This theory functions through the modified boundary condition

$$\mathbf{n} \cdot \boldsymbol{\sigma} = \nabla_S \cdot \boldsymbol{\Sigma} + (\nabla_S \cdot \mathbf{M})\mathbf{n} - (\nabla_S \cdot \mathbf{n})\mathbf{n} \cdot (\nabla_S \cdot \mathbf{M})\mathbf{n} + \mathbf{T}^{(n)}, \tag{4}$$

where \mathbf{n} is the surface normal vector, $\boldsymbol{\sigma}$ the Cauchy stress, ∇_S the surface gradient operator, $\boldsymbol{\Sigma}$ the surface stress, \mathbf{M} the surface bending moment, and $\mathbf{T}^{(n)}$ the traction load.

For the contact interface ($z = 0$) shown in Fig. 1, the nonclassical boundary condition (4) can be materialized (Li and Mi 2019b)

$$\sigma_{xz} + q(x) + k_0 \frac{\partial^2 u_1(x, 0)}{\partial x^2} = 0, \tag{5a}$$

$$\sigma_{zz} + p(x) + \tau_0 \frac{\partial^2 w_1(x, 0)}{\partial x^2} - d_0 \frac{\partial^4 w_1(x, 0)}{\partial x^4} = 0, \tag{5b}$$

where $q_x = \eta p(x)$ and $p(x)$ are the tangential and normal contact pressures, and $u_1(x, 0)$ and $w_1(x, 0)$ denote the tangential and normal displacements on the layer upper surface.

Along the graded layer/substrate interface, perfect bonding condition leads to continuous tractions and displacements

$$\sigma_{xz2}(x, h) = \sigma_{xz1}(x, h), \tag{6a}$$

$$\sigma_{xz2}(x, h) = \sigma_{xz1}(x, h), \tag{6b}$$

$$u_2(x, h) = u_1(x, h), \tag{6c}$$

$$w_2(x, h) = w_1(x, h). \tag{6d}$$

In Fourier space, the general solution of displacements and stresses in an exponentially graded layer has been derived by Yan and Mi (2017), in terms of four unknown functions (B_1 – B_4) of Fourier transform variable (ξ). The elastic fields in a positive half-plane was also given in terms of two unknown function (A_5 and A_6). The boundary conditions (5a, 5b) and (6a–d) provide six equations for determining these six unknown functions. Application of the standard linear algebra algorithm results in

$$B_j(\xi) = (-1)^j \left(\frac{M_{1j}}{M} \tilde{q}(\xi) - \frac{M_{2j}}{M} \tilde{p}(\xi) \right), \quad j = 1, \dots, 4, \tag{7a}$$

$$A_j(\xi) = (-1)^j \left(\frac{M_{1j}}{M} \tilde{q}(\xi) - \frac{M_{2j}}{M} \tilde{p}(\xi) \right), \quad j = 5, 6, \tag{7b}$$

where $\tilde{q}(\xi)$ and $\tilde{p}(\xi)$ stand for the Fourier transforms of the tangential and normal contact pressures exerted on the layer upper surface due to the nanoindentation of the rigid cylinder. In addition, M_{ij} ($i = 1, 2; j = 1 - 6$) denotes the elements of the cofactor matrix to the 6×6 coefficient matrix of the linear algebraic system with the determinant M . They are documented in Appendix A for brevity and easy reference.

Up to this point, the normal contact pressure $p(x)$ is still an unknown. It can be solved by applying the displacement constraint along the contact interface ($z = h$)

$$\frac{\partial w_1}{\partial x} = -\frac{x}{R}, \quad -a \leq x \leq b. \tag{8}$$

The substitution of the displacement along the contact interface into the above equation leads to the integral equation

$$\int_{-a}^b \eta p(t) \varphi_1(x, t) dt + \int_{-a}^b p(t) \varphi_2(x, t) dt = \frac{x}{R}, \quad -a \leq x \leq b, \tag{9}$$

where

$$\varphi_1(x, t) = \frac{1}{\pi} \int_0^{+\infty} IE_1(\xi, 0) \cos(\xi(t - x)) d\xi, \tag{10a}$$

$$\varphi_2(x, t) = \frac{1}{\pi} \int_0^{+\infty} E_2(\xi, 0) \sin(\xi(t - x)) d\xi. \tag{10b}$$

In the above equations, E_1 and E_2 are given by

$$E_1(\xi, 0) = I\xi \sum_{j=1}^4 (-1)^j s_j \frac{M_{1j}}{M}, \tag{11a}$$

$$E_2(\xi, 0) = \xi \sum_{j=1}^4 (-1)^j s_j \frac{M_{2j}}{M}. \tag{11b}$$

Note that, for frictionless nanocontact problems incorporating only surface tension, an explicit expression may be obtained for Eq. (11b) (Long

Table 1 Asymptotic behavior of the infinite integral (10a)

	IE_1	Asymptot.(IE_1)	$\lim_{\xi \rightarrow \infty}(IE_1)$	Asymptot.(10a)
Classical ($\Gamma \neq 1$)	$I\xi \sum_{j=1}^4 s_j(-1)^j \frac{M_{1j}}{M}$	$-\frac{(\kappa-1)}{4\mu_1}$	$-\frac{(\kappa-1)}{4\mu_1}$	$-\frac{(\kappa-1)}{4\mu_1} \delta(t-x)$
Only τ_0 ($\Gamma = 1$)	$-\frac{(\kappa-1)}{\tau_0(\kappa+1)\xi+4\mu_2} a$	$-\frac{(\kappa-1)}{\tau_0(\kappa+1)\xi}$	0	N.A.
Only d_0 ($\Gamma = 1$)	$-\frac{(\kappa-1)}{d_0(\kappa+1)\xi^3+4\mu_2}$	$O(\xi^{-3})$	0	N.A.
Nonclassical ($\Gamma \neq 1$)	$I\xi \sum_{j=1}^4 s_j(-1)^j \frac{M_{1j}}{M}$	$O(\xi^{-4})$	0	N.A.
Nonclassical ($\Gamma = 1$)	$-\frac{(\kappa-1)\mu_2}{\Omega} b$	$O(\xi^{-4})$	0	N.A.

^aFathabadi and Alinia (2020)

$${}^b \Omega = \xi(\kappa + 1)(d_0\xi^2 + k_0 + \tau_0)\mu_2 + k_0\xi^2\kappa(d_0\xi^2 + \tau_0) + 4\mu_2^2$$

Table 2 Asymptotic behavior of the infinite integral (10b)

	E_2	Asymptot.(E_2)	$\lim_{\xi \rightarrow \infty}(E_2)$	Asymptot.(10b)
Classical ($\Gamma \neq 1$)	$\xi \sum_{j=1}^4 s_j(-1)^j \frac{M_{2j}}{M}$	$-\frac{(\kappa+1)}{4\mu_1}$	$-\frac{(\kappa+1)}{4\mu_1}$	$-\frac{(\kappa+1)}{4\pi\mu_1(t-x)}$
Only τ_0 ($\Gamma = 1$)	$-\frac{(\kappa+1)}{\tau_0(\kappa+1)\xi+4\mu_2} a$	$-\frac{1}{\tau_0\xi}$	0	$-\frac{\pi \operatorname{sgn}(t-x)}{2\tau_0\xi}$
Only d_0 ($\Gamma = 1$)	$-\frac{(\kappa+1)}{d_0(\kappa+1)\xi^3+4\mu_2} b$	$-\frac{1}{d_0\xi^3}$	0	N.A.
Nonclassical ($\Gamma \neq 1$)	$\xi \sum_{j=1}^4 s_j(-1)^j \frac{M_{2j}}{M}$	$-\frac{1}{d_0\xi^3}$	0	N.A.
Nonclassical ($\Gamma = 1$)	$-\frac{(\kappa+1)\mu_2-k_0\kappa\xi}{\Omega} c$	$-\frac{1}{d_0\xi^3}$	0	N.A.

^aLong et al. (2012).

^bLi and Mi (2021).

^c

$$\Omega = \xi(\kappa + 1)(d_0\xi^2 + k_0 + \tau_0)\mu_2 + k_0\xi^2\kappa(d_0\xi^2 + \tau_0) + 4\mu_2^2$$

et al. 2012; Le et al. 2021). In the presence of a graded layer possessing Steigmann–Ogden surface effects, it becomes not possible to develop such an analytical expression. Moreover, due to the sliding friction, Eq. (11a) was additionally introduced. This equation does not exist in any frictionless nanocontact problems. The complexity of Eqs. (11a, 11b) makes it impractical to derive an analytical solution for the infinite integrals (10a, 10b). In the literature (Pinyochotiwong et al. 2013; Li and Mi 2019b; Le et al. 2022), numerical quadratures of Gauss-type were employed instead to numerically evaluate these infinite integrals. Because of the critical importance of truncation scheme on integration accuracy and cost, next section makes detailed

investigations on the numerical calculations of the infinite integrals (10a, 10b).

The integral Eq. (9) stands for one of the two governing equations that need to be numerically tackled for the proposed nanocontact problem. The other one is represented by the force equilibrium condition between the externally applied indentation force and the resultant of the contact pressure

$$\int_{-a}^b p(x)dx = P. \tag{12}$$

Under the condition of sliding friction, it is not necessary to consider the force equilibrium along the horizontal direction and the moment equilibrium.

3 Numerical evaluation of infinite integrals

The goal of this section is to develop an accurate algorithm to calculate the dual infinite integral Eqs. (10a, 10b). For this purpose, the asymptotic behavior of their integrands (11a, 11b) were first analyzed, as shown in Tables 1 and 2, respectively. For the graded layer/substrate structure shown in Fig. 1, both the classical and nonclassical cases are analyzed. In addition, following Vasu and Bhandakkar (2016, 2018), the reduced results for the degenerated case of a completely homogeneous half-plane ($\Gamma = 1$) can be employed to speed up the convergence of the dual infinite integrals. For this reason, the asymptotic behavior for this degenerated case and a few others are simultaneously tabulated in the tables. They were evaluated in MAPLE software package and are consistent with those available in the literature. The agreements help to validate the correctness of the asymptotic analysis.

In Tables 1 and 2, $\text{Asymptot}(\cdot)$ denotes the leading term in the asymptotic expansion of its argument, as Fourier transform variable (ξ) approaches to infinity, $\text{sgn}(\cdot)$ is the sign function and $\delta(\cdot)$ stands for the Dirac delta function. Based on literature results regarding the effects of surface material parameters on contact properties and the numerical tests of the present study, the surface tensile stiffness (k_0) alone shows negligible influence. As a result, the separated effects of k_0 on the asymptotic behavior of the infinite integrals (10a, 10b) does not need to be considered.

3.1 Classical case without surface effects

Let us first consider the classical case without any surface effects ($\tau_0 = 0, k_0 = 0, d_0 = 0$). From Tables 1 and 2, both integrands (11a, 11b) possess singular terms as ξ approaches to infinity. Without separating the singular terms, the asymptotic behavior is shown in Fig. 2a and b. It can be observed that both integrands oscillate almost regularly with the increase of ξ .

For reliable calculations of the infinite integrals, singular terms must be extracted from the integrands (Guler and Erdogan 2004, 2007). By using integral

identities involving trigonometric functions and the singular terms, Eqs. (10a, 10b) can be recast into

$$\varphi_1(x, t) = \int_0^{+\infty} [IE_1 - d_1] \cos(\xi(t-x))d\xi + d_1\pi\delta(t-x), \tag{13a}$$

$$\varphi_2(x, t) = \int_0^{+\infty} [E_2 - d_2] \sin(\xi(t-x))d\xi + \frac{d_2}{t-x}, \tag{13b}$$

where d_1 and d_2 denote the strength of singularity

$$d_1 = \frac{-(\kappa - 1)}{4\mu_1}, \tag{14a}$$

$$d_2 = \frac{-(\kappa + 1)}{4\mu_1}. \tag{14b}$$

Figure 3a and b show the asymptotic behavior of the integrands after extracting the singular terms. Both integrands decay rapidly with ξ . Under such a condition, the infinite upper bound in (13a, 13b) may be safely truncated by a small number. After that, an accurate numerical solution can be obtained with the aid of Gauss–Legendre quadrature. Based on extensive tests, the upper bound is chosen as 500. The further substitution of (13a, 13b) back into the governing integral Eq. (9) leads to

$$\omega p(x) + \frac{1}{\pi} \int_{-a}^b \frac{p(t)}{t-x} dt + \frac{1}{\pi} \int_{-a}^b \psi(x, t)p(t)dt = \frac{x}{Rd_2}, \tag{15}$$

where

$$\psi(x, t) = \eta \int_0^{+\infty} \left[\frac{IE_1 - d_1}{d_2} \right] \cos(\xi(t-x))d\xi + \int_0^{+\infty} \left[\frac{E_2 - d_2}{d_2} \right] \sin(\xi(t-x))d\xi, \tag{16a}$$

$$\omega = \frac{\eta d_1}{d_2}. \tag{16b}$$

It is noted that Eq. (15) belongs to the Fredholm integral equation of the second kind. Moreover, it is a singular integral equation of the Cauchy type, as indicated by the second term of its left-hand side.

3.2 Nonclassical case with surface tension only

Next, we aim at investigating the asymptotic behavior of the infinite integrals in the presence of surface effects. As can be observed from Tables 1 and 2, both integrands (11a, 11b) tend to zero as ξ approaches to infinity for all four nonclassical cases. Therefore, there are no singular terms. However, the integrands of infinite integrals (10a, 10b) continuously oscillate from zero to a very large upper bound. The rate of convergence is thus very slow. Some mathematical manipulations may be conducted to optimize the convergence properties. When only surface tension (τ_0) is taken into account, the asymptotic behavior of the integrands in Eqs. (10a, 10b) are presented in Fig. 4a and b. It can be observed that, although the integrands behave oscillatory decaying with ξ , the convergence is very slow.

To speed up the convergence rate, the asymptotic values of IE_1 and E_2 corresponding to a completely homogeneous half-plane ($\Gamma = 1$) may be extracted from the original integrands. For such a particular condition, the infinite integral of the product between Asymptot. (E_2) and sine function has a closed-form solution: $-\int_0^{+\infty} (1/(\tau_0\xi)) \sin[\xi(x-t)] = -\pi/(2\tau_0\xi) \text{sgn}(t-x)$. As a result, the asymptotic value ($-1/(\tau_0\xi)$) of E_2 may be set as the separation term. Although no corresponding analytical solution can be found for IE_1 , the same algorithm may be employed. Following such a reasoning, the infinite integrals (10a, 10b) may

be rewritten in the following forms that are ready for numerical evaluation

$$\begin{aligned} \varphi_1(x, t) = & \frac{1}{\pi} \int_0^{+\infty} [IE_1 - IE_1|_{homo}] \cos(\xi(t-x))d\xi \\ & + \frac{1}{\pi} \int_0^{+\infty} IE_1|_{homo} \cos(\xi(t-x))d\xi, \end{aligned} \tag{17a}$$

$$\begin{aligned} \varphi_2(x, t) = & \frac{1}{\pi} \int_0^{+\infty} \left[E_2(\xi, 0) + \frac{1}{\tau_0\xi} \right] \sin(\xi(t-x))d\xi \\ & - \frac{\text{sgn}(t-x)}{2\tau_0\xi}, \end{aligned} \tag{17b}$$

where the subscript “homo” denotes the reduced solution of IE_1 corresponding to a completely homogeneous half-plane ($\Gamma = 1$). In Fig. 5a and b, we present the asymptotic behavior of the integrands in the first infinite integrals in the right-hand side of Eqs. (17a, 17b). As before, the infinite upper bound was set as 500 and Gauss–Legendre quadrature was employed for the numerical integration. In contrast to Fig. 4a and b, both integrands decay rapidly after the separation. In particular, Fig. 5b shows a more rapid convergence.

In addition, the second infinite integral on the right-hand side of Eq. (17a) can also be analytically integrated

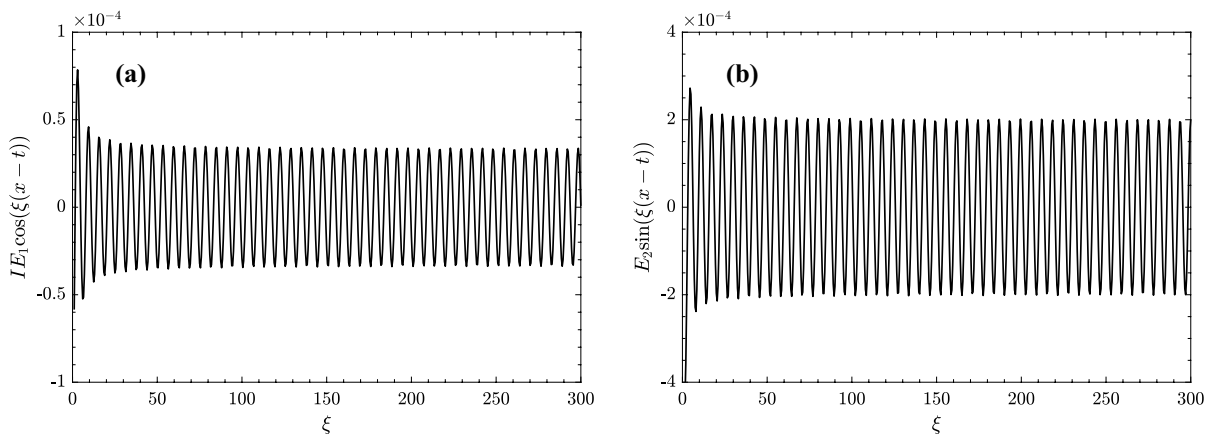


Fig. 2 Asymptotic behavior of the integrands in the infinite integrals (10a, 10b), without separating the singular terms ($\tau_0 = 0, k_0 = 0, d_0 = 0$)

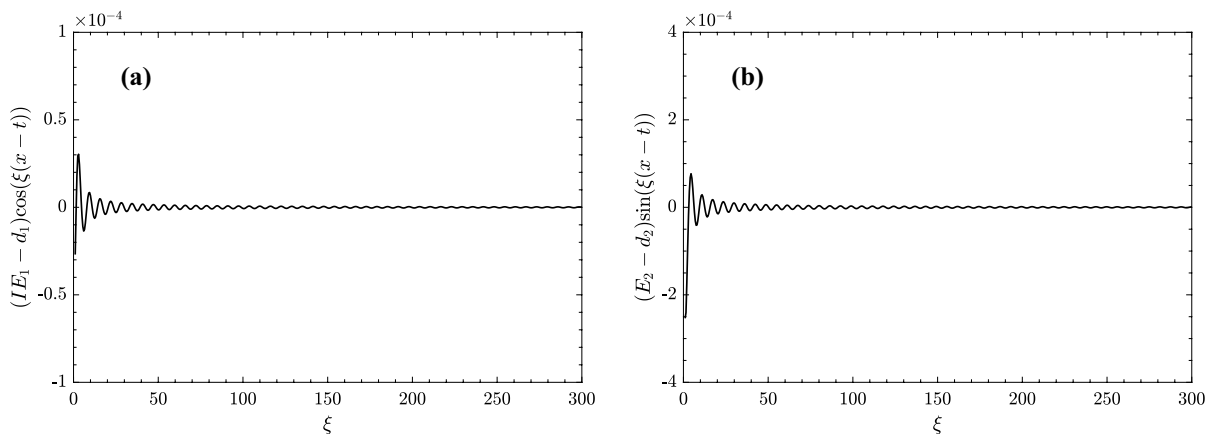


Fig. 3 Asymptotic behavior of the integrands in the infinite integrals (10a, 10b), after separating the singular terms ($\tau_0 = 0, k_0 = 0, d_0 = 0$)

$$\frac{1 - \kappa}{\pi \tau_0 (1 + \kappa)} [-\sin(|t - x|\varpi)\text{si}(|t - x|\varpi) - \cos(|t - x|\varpi)\text{ci}(|t - x|\varpi)], \tag{18}$$

where

$$\varpi = \frac{4\mu_2}{\tau_0(\kappa + 1)}, \tag{19}$$

and $\text{si}(\cdot)$ and $\text{ci}(\cdot)$ are sine and cosine integrals.

3.3 Nonclassical case with surface flexural rigidity only

In this subsection, we analyze the asymptotic behavior of the integrands in Eqs. (10a, 10b) when only surface flexural rigidity (d_0) is considered. Fig. 6a and b show the asymptotic behavior as Fourier transform variable (ξ) grows from zero to 300. The declining rate of the oscillatory integrands is quite slow. This behavior makes it nearly impossible to truncate the infinite upper bound of the improper integrals with a reasonably large number.

To accelerate the convergence rate, the infinite integrals (10a, 10b) can be recast in the form of

$$\varphi_1(x, t) = \frac{1}{\pi} \int_0^{+\infty} [IE_1 - IE_1|_{\text{homo}}] \cos(\xi(t - x))d\xi + \frac{1}{\pi} \int_0^{+\infty} IE_1|_{\text{homo}} \cos(\xi(t - x))d\xi, \tag{20a}$$

$$\varphi_2(x, t) = \frac{1}{\pi} \int_0^{+\infty} [E_2 - E_2|_{\text{homo}}] \sin(\xi(t - x))d\xi + \frac{1}{\pi} \int_0^{+\infty} E_2|_{\text{homo}} \sin(\xi(t - x))d\xi. \tag{20b}$$

This is equivalent to separate the values of IE_1 and E_2 corresponding to a completely homogeneous half-plane ($\Gamma = 1$). When only the surface flexural rigidity is considered, the second term on the right-hand side of Eqs. (20a, 20b) can be analytically evaluated

$$-\frac{\sqrt{3}(\kappa-1)}{4\pi^{3/2}\mu_2(t-x)} \text{MeijerG}\left(\frac{1}{2}, [], \left[\frac{1}{6}, \frac{1}{2}, \frac{1}{2}, \frac{5}{6}, 1\right], \left[\frac{1}{3}, \frac{2}{3}\right], \frac{(t-x)^6 \mu_2^2}{2916d_0^2(\kappa+1)^2}\right), \tag{21a}$$

$$-\frac{\sqrt{3}(\kappa+1)}{4\pi^{3/2}\mu_{20}(t-x)} \text{MeijerG}\left(1, [], \left[\frac{1}{3}, \frac{1}{2}, \frac{2}{3}, 1, 1\right], \left[\frac{1}{6}, \frac{5}{6}\right], \frac{(t-x)^6 \mu_{20}^2}{2916d_0^2(\kappa+1)^2}\right), \tag{21b}$$

where $\text{MeijerG}(\cdot)$ stands for the Meijer's G-function whose definition and main properties can be found in Gradshteyn and Ryzhik (2015).

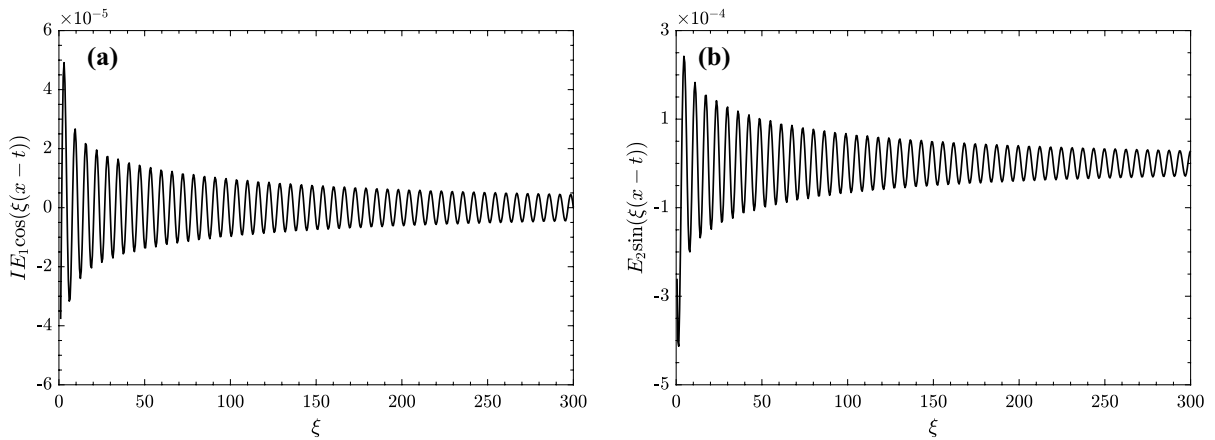


Fig. 4 Asymptotic behavior of the integrands in the infinite integrals (10a, 10b), without separation ($\tau_0 \neq 0, k_0 = 0, d_0 = 0$)

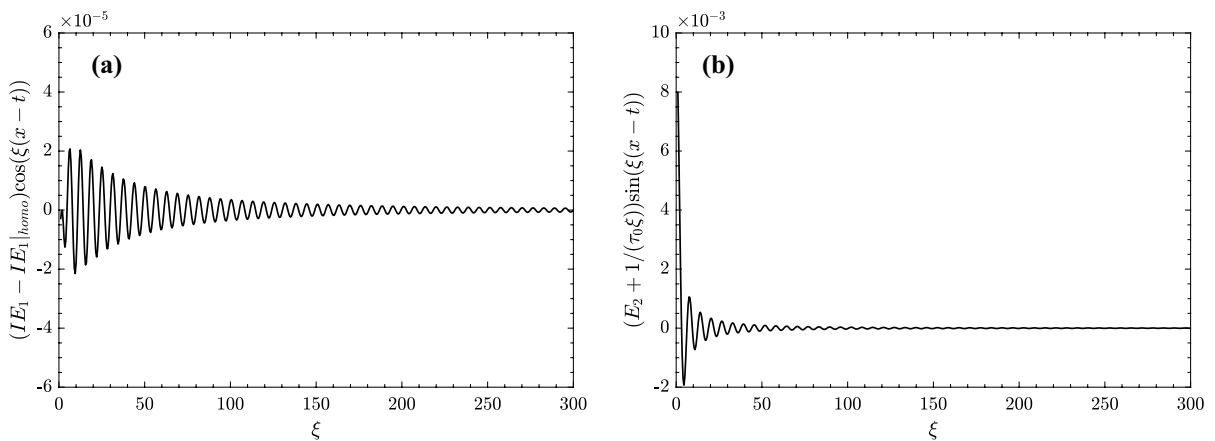


Fig. 5 Asymptotic behavior of the integrands in the infinite integrals (10a, 10b), after separating the solutions corresponding to a completely homogeneous half-plane ($\tau_0 \neq 0, k_0 = 0, d_0 = 0$)

In Fig. 7a and b, we show the asymptotic behavior of the integrands belonging to the first infinite integrals on the right-hand side of Eqs. (20a, 20b). After the separation of the corresponding completely homogeneous half-plane solutions, both integrands decay very rapidly with the increase of ξ . Based on this observation, it has become possible to truncate the infinite upper bound with a reasonably large number (500). After that, Gauss–Legendre quadrature is employed to evaluate the finite integral.

3.4 Nonclassical case with full Steigmann–Ogden surface effects

When the full Steigmann–Ogden surface theory is accommodated, the same separation scheme can still be used. As a result, Eqs. (20a, 20b) remain effective. Similar to previous three cases studied in the present section, the integrands of the infinite integrals (10a,

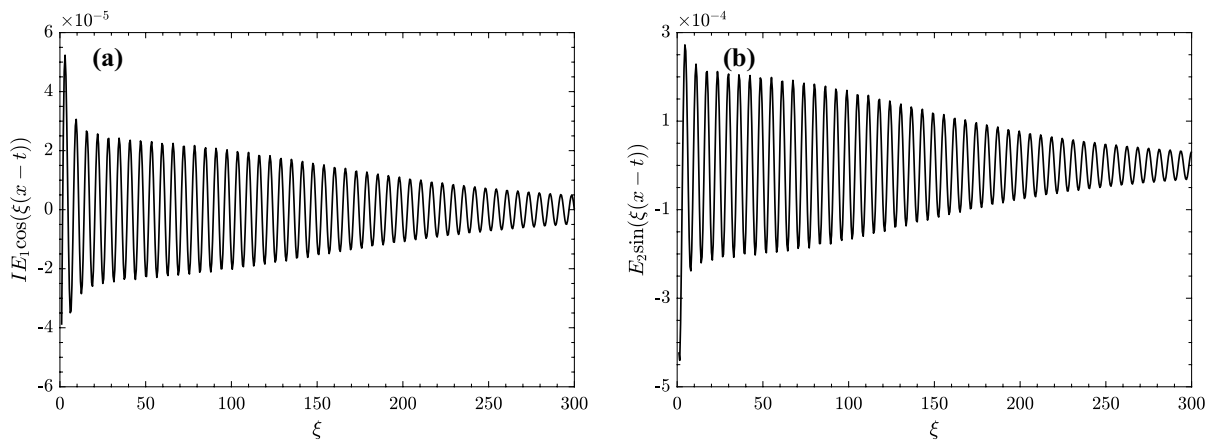


Fig. 6 Asymptotic behavior of the integrands in the infinite integrals (10a, 10b), without separation ($\tau_0 = 0, k_0 = 0, d_0 \neq 0$)

10b) oscillates and decay slowly with the integration variable ξ (Fig. 8a and b).

After separating the corresponding homogeneous half-plane solutions of the integrands, much faster rate of decay can be identified (Fig. 9a and b). When compared with the nonclassical cases considering only surface tension or surface flexural rigidity, both integrands decay faster and nearly converge to zero as $\xi \rightarrow 300$. As before, Gauss–Legendre quadrature can be used to evaluate the infinite integrals after the proper separation of integrands. The upper bound of the infinite integrals are truncated as 500. It is sufficient to accurately evaluate the first infinite integrals in Eqs. (20a, 20b). However, analytical solutions cannot be found for the second infinite integrals anymore. Numerical integration must also be used. They are numerically evaluated by using the built-in “integral” function available in MATLAB. The upper bound of the integration interval was directly set as positive infinity.

4 Numerical solution algorithm

In this section, we develop an efficient solution algorithm to the integral Eqs. (9), (12) and (15). To proceed, let us first make the following replacements of variables

$$t = \frac{b+a}{2}r + \frac{b-a}{2}, \quad x = \frac{b+a}{2}s + \frac{b-a}{2}, \quad (22a,b)$$

$$\phi(r) = \frac{p(r)}{P/h}. \quad (22c)$$

Since both x and t are defined within the contact zone $[-a, b]$, the transformed variables r and s have the closed interval $[-1, 1]$. Function $\phi(r)$ is the dimensionless form of the contact pressure.

4.1 Numerical scheme for the classical case

For the classical case without any surface effects, Eqs. (15) and (12) can be converted into the following expressions with the help of the dimensionless quantities defined in (22a–c)

$$\begin{aligned} \frac{\eta\phi(s)d_1}{d_2} + \frac{1}{\pi} \int_{-1}^1 \frac{\phi(r)}{r-s} dr + \frac{1}{\pi} \int_{-1}^1 \psi^*(s,r)\phi(r)dr \\ = \frac{(b+a)s + (b-a)}{2Rd_2P/h}, \quad -1 \leq s \leq 1, \end{aligned} \quad (23a)$$

$$\frac{b+a}{2h} \int_{-1}^1 \phi(r)dr = 1, \quad (23b)$$

where

$$\psi^*(s,r) = \frac{(b+a)}{2}\psi(s,r). \quad (24)$$

The singularity index of the integral Eq. (23a) is -1 , since the contact pressure is zero and therefore bounded at both contact boundaries (Erdogan and

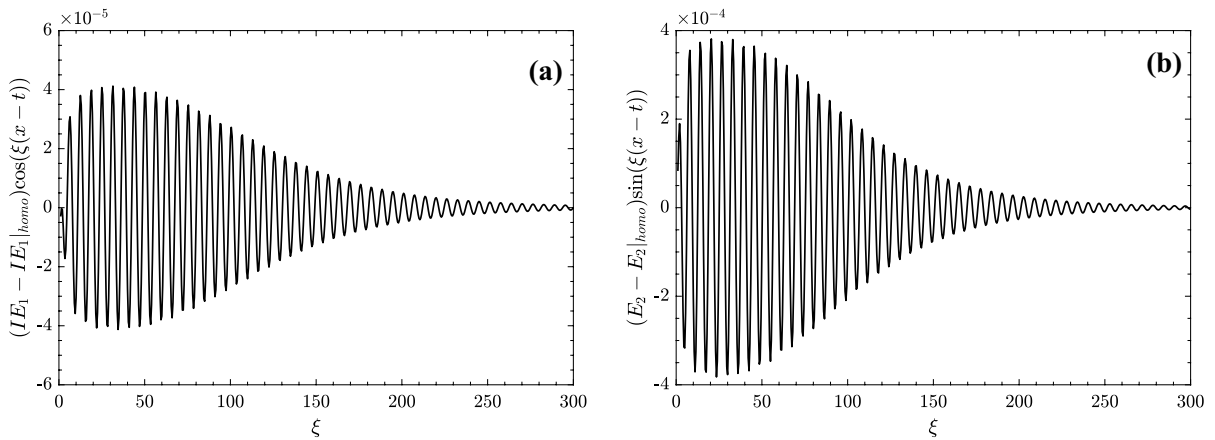


Fig. 7 Asymptotic behavior of the integrands in the infinite integrals (10a, 10b), after separating the solutions corresponding to a completely homogeneous half-plane ($\tau_0 = 0, k_0 = 0, d_0 \neq 0$)

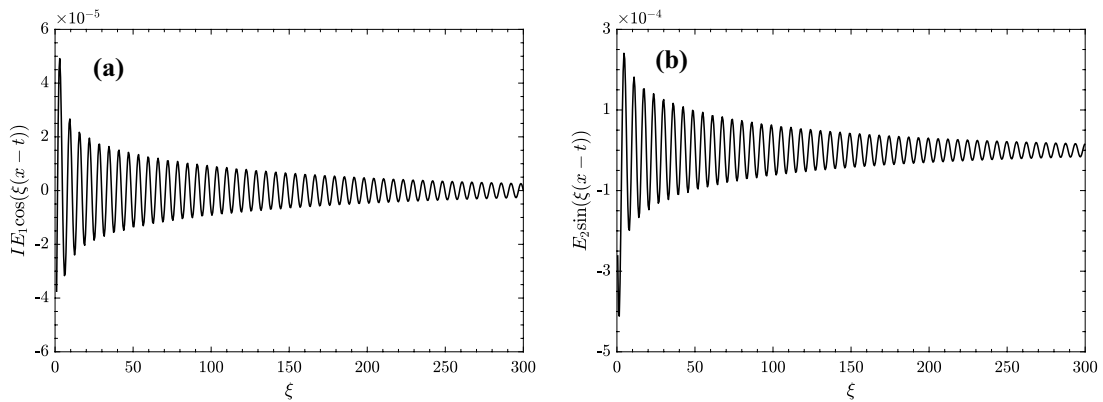


Fig. 8 Asymptotic behavior of the integrands in the infinite integrals (10a, 10b), without separation ($\tau_0 \neq 0, k_0 \neq 0, d_0 \neq 0$)

Gupta 1972). As a result, the dimensionless contact pressure $\phi(r)$ may be expressed as

$$\phi(r) = g(r)\delta(r), \tag{25}$$

where $\delta(r)$ is the weight function given by

$$\delta(r) = (1 - r)^\alpha(1 + r)^\beta. \tag{26}$$

In the above equation, the powers α and β are given by

$$\alpha = \frac{1}{2\pi I} \ln \left(\frac{\omega - I}{\omega + I} \right) + N, \tag{27a}$$

$$\beta = -\frac{1}{2\pi I} \ln \left(\frac{\omega - I}{\omega + I} \right) + M, \tag{27b}$$

where N and M can be arbitrary integers. In addition, the following relation should also be satisfied

$$\chi = -(\alpha + \beta) = -(N + M) = -1. \tag{28}$$

Following Erdogan et al. (1973), Gauss–Jacobi quadratures are now employed to discretize and collocate the integral Eqs. (23a, 23b)

$$\sum_{m=1}^N W_m^N g(r_m) \left[\frac{1}{r_m - s_k} + \psi(r_m, s_k) \right] = \frac{(b + a)s_k + (b - a)}{2Rd_2P/h}, \tag{29a}$$

$$k = 1, 2, \dots, N + 1,$$

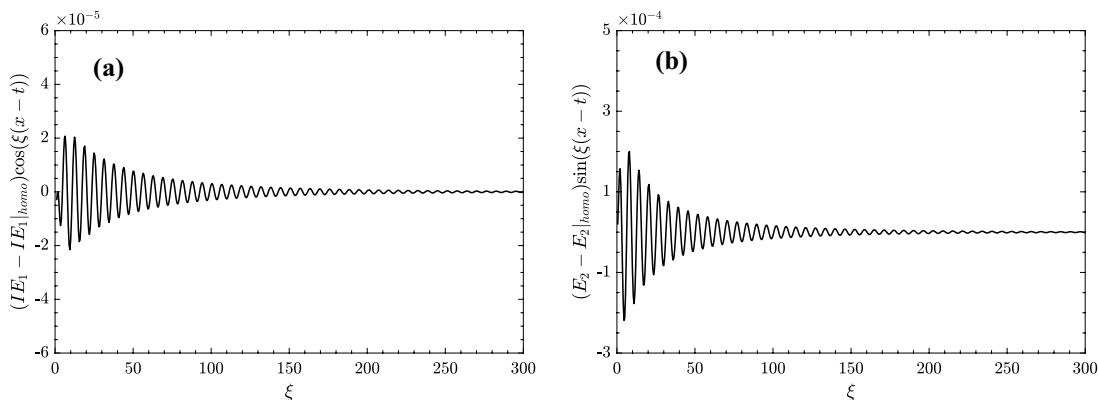


Fig. 9 Asymptotic behavior of the integrands in the infinite integrals (10a, 10b), after separating the solutions corresponding to a completely homogeneous half-plane ($\tau_0 \neq 0, k_0 \neq 0, d_0 \neq 0$)

$$\frac{b+a}{2h} \sum_{m=1}^N W_m^N g(r_m) = \frac{1}{\pi}, \tag{29b}$$

where r_m and s_k are the roots of the associated Jacobi polynomials and W_m^N are the weights of quadratures

$$P_N^{(\alpha,\beta)}(r_m) = 0, \quad m = 1, 2, \dots, N, \tag{30a}$$

$$P_{N+1}^{(-\alpha,-\beta)}(s_k) = 0, \quad k = 1, 2, \dots, N+1, \tag{30b}$$

$$W_m^N = -2^{-\chi} \frac{\Gamma(\alpha)\Gamma(1-\alpha)}{\pi} \frac{P_{N-\chi}^{(-\alpha,-\beta)}(r_m)}{P_N^{(\alpha,\beta)'}(r_m)}. \tag{30c}$$

Equations (29a, 29b) contain $N + 2$ equations for the total number of $N + 2$ unknowns, including the N discretized contact pressures $g(r_m)$ ($m = 1, 2, \dots, N$) and the two contact boundaries a and b . Although this algebraic system is linear to the contact pressures $g(r_m)$, it is nonlinear about the contact boundaries a and b . Therefore, an iterative scheme needs to be implemented. An effective iterative algorithm for determining these unknowns has been developed by Comez and Erdol (2013) and is also adopted in the present work to solve the classical contact pressures and contact boundaries without surface effects.

4.2 Numerical scheme for the nonclassical case

By the use of equations (22a–c), the integral Eqs. (9) and (12) can be expressed as

$$\frac{1}{\pi} \int_{-1}^1 \psi^*(s, r) \phi(r) dr = \frac{(b+a)s + (b-a)}{2RP/h}, \quad -1 \leq s \leq 1, \tag{31a}$$

$$\frac{b+a}{2h} \int_{-1}^1 \phi(r) dr = 1, \tag{31b}$$

where

$$\psi^*(s, r) = \frac{b+a}{2} \psi(s, r), \tag{32a}$$

$$\psi(s, r) = \eta \varphi_1(s, r) + \varphi_2(s, r). \tag{32b}$$

In the presence of surface effects, the contact pressures at both contact boundaries are not zero anymore. However, they are still bounded. As a result, the singularity index of the integral Eq. (31a) is still -1 (Erdogan and Gupta 1972). Following Erdogan and Gupta (1972), we may employ Gauss–Chebyshev quadrature of the second kind to discretize the definite integral in (31a). In the meantime, we use Gauss–Chebyshev quadrature of the first kind to collocate this integral equation

$$\sum_{m=1}^N \frac{(1-r_m^2)}{N+1} g(r_m) \psi(r_m, s_k) = \frac{(b+a)s_k + (b-a)}{2RP/h}, \quad k = 1, 2, \dots, N+1, \tag{33a}$$

$$\frac{b+a}{2h} \sum_{m=1}^n \frac{(1-r_m^2)}{N+1} g(r_m) = \frac{1}{\pi}, \quad (33b)$$

where

$$g(r_m) = \frac{\phi(r_m)}{\sqrt{(1-r_m^2)}}, \quad (34a)$$

$$r_m = \cos\left(\frac{m\pi}{N+1}\right), \quad m = 1, 2, \dots, N, \quad (34b)$$

$$s_k = \cos\left(\frac{\pi(2k-1)}{2(N+1)}\right), \quad k = 1, 2, \dots, N+1. \quad (34c)$$

Similar to Eqs. (29a, 29b), the algebraic system (33a, 33b) also contains $N+2$ equations for the determination of the $N+2$ unknowns. They are composed of the discretized contact pressures $g(r_m)$ ($m = 1, 2, \dots, N$) and both contact boundaries a and b . Again, the algebraic system is linear about the contact pressures, but nonlinear to the contact boundaries. To determine these unknowns, an iterative algorithm is needed. Note that (33a) has $N+1$ equations. When using them to determine the N contact pressures $g(r_m)$, anyone of them can be extracted and combined with (33b). As the first step, initial values of both contact boundaries (a and b) are proposed. Second, the N discretized contact pressures $g(r_m)$ are evaluated from Eq. (33a), by excluding anyone from the $N+1$ collocated equations. The standard algorithm is sufficient for this linear algebraic system. Third, the just solved contact pressures $g(r_m)$ are substituted into Eq. (33b) and the equation that was previously excluded from (33a). The residual errors of both equations are then calculated. Provided that both errors are less than or equal to 10^{-6} , solutions deem to be found. Otherwise, both contact boundaries a and b need to be updated, by following the method of steepest descent, and the loop needs to be recycled again from the second step.

5 Results and discussion

We have presented the formulation and method of solution for the sliding frictional nanocontact problem between a rigid cylinder and an exponentially graded layer/substrate structure. The governing integral equations were converted into an algebraic

system of equations for determining the asymmetric nanocontact pressures and boundaries. In this section, we conduct parametric studies with respect to surface properties, sliding frictional coefficient, and the gradient index of the layer modulus.

5.1 Validation of the solution algorithm

Since the classical case without surface effects has been studied in the literature (Guler and Erdogan 2007), it is beneficial to first verify and validate the accuracy of the developed method of solution and numerical algorithm (Sect. 4.1). Figs. 10a and b show the contact pressure distributions for the frictionless ($\eta = 0$) and sliding frictional ($\eta = 0.7$) conditions, respectively. Three shear moduli ratios are considered, standing for a hard ($\Gamma = 1/7$), a homogeneous ($\Gamma = 1$) and a soft ($\Gamma = 7$) layer. From Eq. (2), defining Γ is equivalent to assigning the gradient index βh of the layer modulus. For all six cases, the agreement between our results and the literature data is perfect. This indicates the reliability of our method of solution (Sect. 4.1). In general, the maximum contact pressure corresponding to the soft layer ($\Gamma = 7$) is much larger than that of the hard one ($\Gamma = 1/7$). As expected, under the frictionless condition, the maximum pressure occurs at the center of the contact zone. For the frictional cases ($\eta = 0.7$), the maximum contact pressure deviates appreciably from the center.

Next, let us verify and validate the method of solution and numerical algorithm for the nonclassical case (Sect. 4.2). For the nanocontact between a completely homogeneous half-plane and a rigid cylinder, Long et al. (2012) studied the sole influence of surface tension (τ_0). In Fig. 11, we compared our results with the contact pressures extracted from Long et al. (2012), by considering the surface tension only. The classical solutions without surface tension are also presented. Note that, in the dimensionless form, the classical contact pressure has nothing to do with the radius of the rigid cylinder. For all six cases, our results agree perfectly with the literature data, indicating the reliability of our solution algorithm for the nonclassical scenario (Sect. 4.2).

5.2 Contact pressure and contact boundaries

Now, let us investigate the contact pressure distribution and contact boundaries under the influence of surface properties, shear moduli ratio and sliding

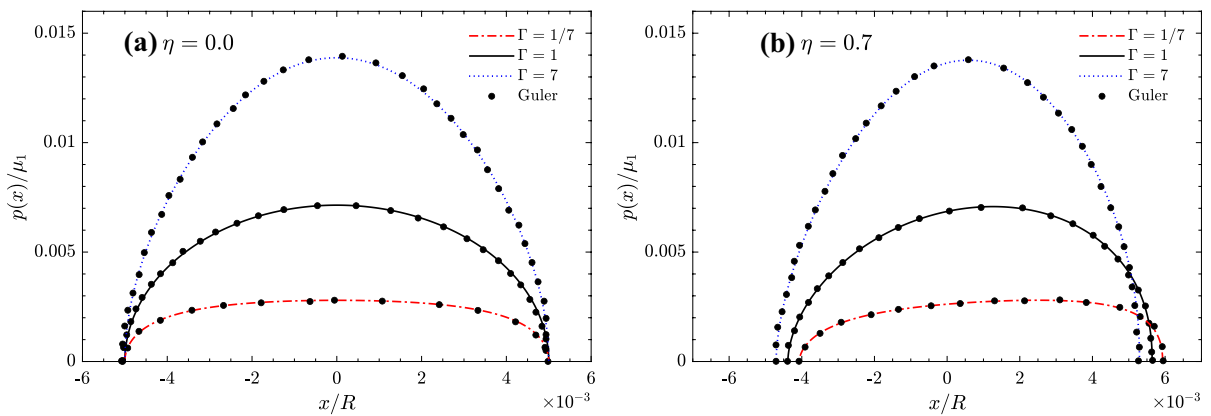


Fig. 10 Validation of the contact pressures with respect to Guler and Erdogan (2007) for the classical case without any surface effects. Two sliding frictional coefficients and three shear moduli ratios are considered ($R/h = 100$, $(b + a)/R = 0.01$, $\Gamma = \mu_2/\mu_1$)

frictional coefficient. In particular, the effects of three Steigmann–Ogden surface parameters are emphasized. The shear modulus of the substrate and Poisson’s ratio of both deformable media are fixed as $\mu_2 = 1$ MPa and $\nu = 0.4$ (Long et al. 2012; Long and Wang 2013). The other parameters are taken as $h = 1$ μm , $R = 100$ μm and $P = 10\text{nN}$.

Figure 12 shows the effects of separate surface parameters on contact pressure and contact boundaries. As aforementioned, since the effects of surface tensile stiffness is very marginal, only surface tension and surface flexural rigidity are considered, when investigating the effects of individual surface parameters. Therefore, only τ_0 and d_0 are considered separately in the current example. Three different magnitudes of either parameter are considered. The classical solutions are also presented for easy comparisons. The other variables are given in the captions of the figures.

From Fig. 12, both surface tension and surface flexural rigidity significantly affect the distribution pattern of the contact pressure. For either parameter, the maximum contact pressure occurs near the midpoint of the contact zone and decays monotonically toward the contact boundaries. In the presence of surface effects, the minimum contact pressure taking place at both contact boundaries becomes nonzero. Furthermore, with the inclusion of sliding friction, the contact pressure is not symmetric about the symmetry

axis (z) of the rigid cylinder anymore. The contact pressure at the left boundary is always larger than that of the right boundary. The effects of surface tension are more significant than those of surface flexural rigidity with the equal magnitude. When only considering surface flexural rigidity, the maximum contact pressure slightly decreases with its increased magnitude. In contrast, with the increased surface tension, the maximum contact pressure increases obviously and the contact interval shrinks continuously.

Having explored the individual effects of surface tension and surface flexural rigidity, let us now consider the complete Steigmann–Ogden surface theory. We define a dimensionless parameter α to represent the equal magnitude of three independent Steigmann–Ogden surface parameters (τ_0, k_0, d_0). In the subsequent parametric analysis, three levels of α will be considered (Table 3).

Figure 13 shows the dimensionless contact pressure for three levels of the dimensionless parameter α denoting the equal magnitude of τ_0, k_0 and d_0 . The classical solution is also presented for comparison purpose. The common effects of the three surface parameters on contact pressure are similar to that of only considering surface tension (Fig. 12). This indicates that surface tension plays a leading role. For all four cases, the maximum pressures are near the center of the contact zone. The loss of symmetry about the z -axis is apparently due to the presence of sliding

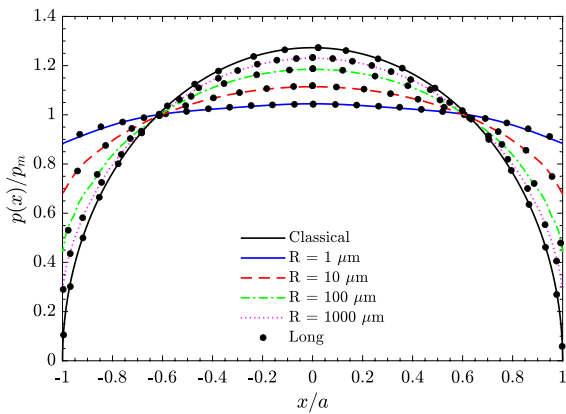


Fig. 11 Validation of the contact pressure between a completely homogeneous half-plane and a rigid cylindrical indenter under the sole influence of surface tension (Long et al. 2012). Four indenter radii are considered ($\Gamma = 1$, $\mu_1 = \mu_2 = 1$ MPa, $\nu = 0.4$, $\eta = 0$, $\tau_0 = 0.1$ nN/nm, $P = 10$ nN/ μm , $p_m = P/(b + a)$)

friction. Furthermore, the maximum contact pressure increases with the dimensionless parameter α . Governed by the conservation of the external indentation force, an opposite trend can be observed for the contact size. Except the classical case, the contact pressure at both contact boundaries becomes nonzero. For all nonclassical curves, the contact pressure at the right boundary is slightly lower than that at the left boundary.

Next, let us investigate the effects of sliding frictional coefficient η . Figure 14 shows the contact pressure for three frictional coefficients. The sliding frictional coefficient significantly affects the distribution symmetry of the contact pressure. With the increased frictional coefficient, the contact pressure at the left contact boundary increases apparently. An opposite trend can be found for the right contact boundary. As a result, for a nonzero frictional coefficient, the minimum pressure always takes place at the right boundary of the contact zone. In addition, the contact zone continuously deviates toward the sliding frictional direction with the increased η . While the sliding frictional coefficient greatly affects the distribution pattern of the contact pressure, the maximum

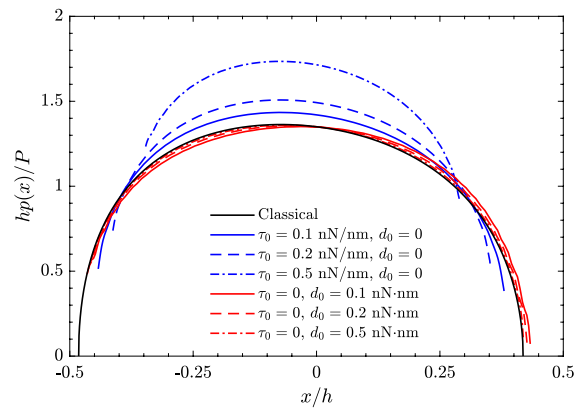


Fig. 12 Distribution of contact pressure between the graded layer and the rigid cylindrical indenter for three levels of surface tension or surface flexural rigidity ($\eta = 0.4$, $\Gamma = 1/3$)

contact pressure is much less influenced (Fathabadi and Alinia 2020).

Figure 15 shows the effects of the shear moduli ratio or equivalently the gradient index on contact pressure and contact boundaries. Five shear moduli ratios are considered. They represent two hard graded layers ($\Gamma = 1/6, 1/3$), two soft graded layers ($\Gamma = 3, 6$) and one completely homogeneous layer ($\Gamma = 1$). For the sliding frictional coefficient $\eta = 0.4$, the maximum contact pressures still take place near the center of the contact zone and the minimum contact pressure always occurs at the right contact boundary. With the increased shear moduli ratio, the maximum contact pressure decays monotonically and the contact zone expands appreciably.

5.3 Stresses and displacements along the contact interface

The previous subsection examined the effects of Steigmann–Ogden surface parameters, shear moduli ratio and sliding frictional coefficient on contact pressures and contact boundaries. Nevertheless, their effects on displacements and stresses along the contact interface have not been studied. This is the objective of the current subsection. Following Eqs. (29b)

Table 3 Definition of the dimensionless parameter α representing the equal magnitude of three Steigmann–Ogden surface parameters (τ_0, k_0 and d_0)

α	τ_0 (nN/nm)	k_0 (nN/nm)	d_0 (nN·nm)
0.1	0.1	0.1	0.1
0.2	0.2	0.2	0.2
0.5	0.5	0.5	0.5

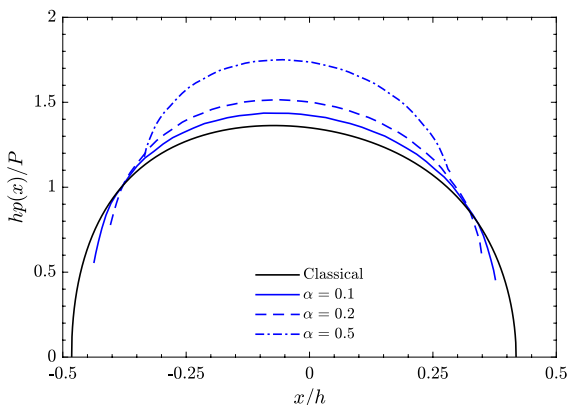


Fig. 13 Distribution of contact pressure between the graded layer and the rigid cylindrical indenter for three levels of the dimensionless parameter α ($\eta = 0.4, \Gamma = 1/3$)

and (33b), the tangential and normal contact pressures in Fourier space can be expressed by

$$\tilde{q}(\xi) = \eta \tilde{p}(\xi), \quad \tilde{p}(\xi) = \frac{(a+b)P}{2h} \sum_{m=1}^N T_m^N g(r_m) e^{I \xi r_m (a+b)/2}. \tag{35a,b}$$

For the classical case without surface elasticity

$$T_m^N = -\frac{\Gamma(\alpha)\Gamma(1-\alpha)}{2\pi} \frac{P_{N-\chi}^{(-\alpha,-\beta)}(r_m)}{P_N^{(\alpha,\beta)'}(r_m)}. \tag{36}$$

For the nonclassical case

$$T_m^N = \frac{1-r_m^2}{N+1}. \tag{37}$$

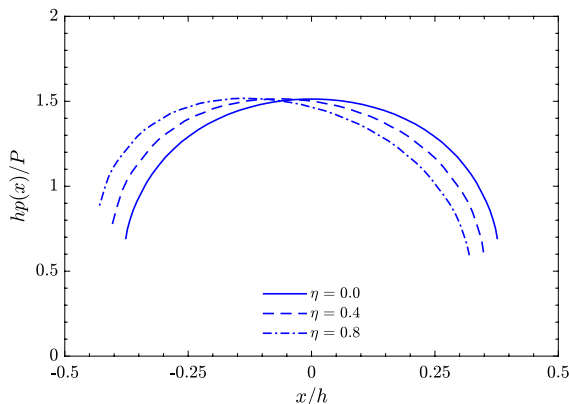


Fig. 14 Distribution of contact pressure between the graded layer and the rigid cylindrical indenter for three frictional coefficients ($\alpha = 0.2, \Gamma = 1/3$)

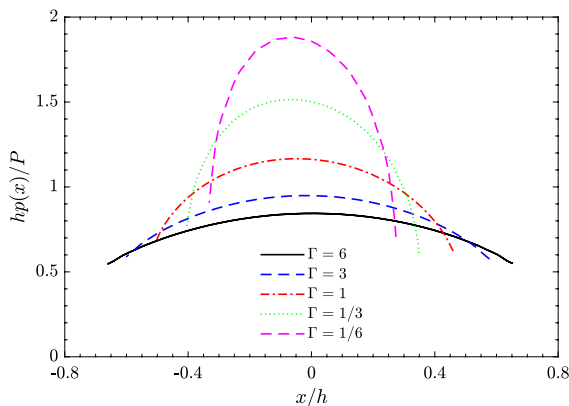


Fig. 15 Distribution of normalized contact pressure between the graded layer and the rigid cylinder for five shear moduli ratios ($\alpha = 0.2, \eta = 0.4$)

To proceed, we need to first substitute the contact pressures in Eqs. (35a,b) back into the expressions (7a, 7b). After that, the displacements and stresses in the transformed space can be evaluated. Finally, their inverse Fourier transforms lead to the displacements and stresses in the physical space. Once the contact pressures along the contact surface are obtained, the subsequent calculation process is

not different from the analysis of a nanocontact problem loaded by surface tractions.

Figure 16a–d show the distribution of normal stress, shear stress, tangential stress and subsidence displacement along the contact interface ($z = 0$). Three levels of the dimensionless parameter α are considered. The classical solutions are also presented. For contact stresses shown in Fig. 16a–c, the peak values of the normalized stresses decay with the inclusion of surface effects. Furthermore, the very sharp transitions of the classical stress curves are significantly relaxed, due to the presence of surface effects. This phenomenon means that Steigmann–Ogden surface theory helps to reduce the impractical stress singularities that are inherent to the classical theory of elasticity.

With the increased α , the maximum normal and tangential stresses continuously decrease. The position of peak shear stress deviates toward the opposite direction of the sliding friction. Resulting from the semiinfinity of the layer/substrate structure, the subsidence displacement shown in Fig. 16d can only be presented with respect to a reference position $x_0/h = 3$ (Li and Mi 2021). From Fig. 16d, the extreme value of the subsidence displacement decreases with the increased α . Also, due to the presence of sliding friction, the displacement at $x/h = -3$ becomes nonzero.

Figure 17a–d show the effects of sliding frictional coefficient (η) on the contact stresses and the subsidence displacement. Based on these figures, the inclusion of sliding friction results in asymmetric distribution of all contact fields. With the increased η , the contact zone deviates toward the direction of the applied tangential force. For the normal stress shown in Fig. 17a, the extreme value decreases with the increased η . An opposite trend can be observed for the shear stress (Fig. 17b) and the tangential stress (Fig. 17c). In Fig. 17b, the shear stress appears at the contact interface for $\eta = 0$, due to the presence of surface effects. For the subsidence displacement shown in Fig. 17d, the peak value near the midpoint of the contact zone continuously decreases with the increased sliding frictional coefficient.

Figure 18a–d show the contact stresses and subsidence displacement along the contact interface for five shear moduli ratios. The maximum stresses appearing in Fig. 18a–c decrease with the shear moduli ratio. However, the increase of shear moduli ratio leads to appreciably larger subsidence displacement (Fig. 18d). Due to the presence of sliding friction, the relative displacement at $x/h = -3$ becomes nonzero.

The classical normal and shear stress curves possess sharp corners at both contact boundaries (Fig. 16a and b). In the presence of surface effects, the sharp corners disappear. Smooth transitions of normal and shear stresses are found for all five shear moduli ratios. Furthermore, the softer the graded layer is, the more smooth the normal and shear stresses at the contact boundaries become (Fig. 18a and b).

5.4 Stresses and displacements inside the graded layer

In this subsection, let us investigate the distribution of vertical stress and subsidence displacement inside a hard graded layer ($\Gamma = 1/3$). Figure 19a and b show the contour plots of the vertical stress for the classical ($\alpha = 0$) and the nonclassical ($\alpha = 0.5$) cases, respectively. In the presence of sliding friction ($\eta = 0.4$), the distribution of the vertical stress becomes obviously asymmetric. By comparing the two subfigures, it is clear that the maximum vertical stress near the midpoint of the contact zone decreases apparently with the inclusion of surface effects. Moreover, an obviously smaller stress concentration can be found below the rigid cylinder. These phenomena indicate that surface effects help the graded layer/substrate structure to alleviate the stress concentrations and thus to elevate the loading capacity.

Figure 20a and b present the contour plots of the subsidence displacement inside a hard graded layer with the shear modulus $\Gamma = 1/3$. Two magnitudes of the dimensionless surface parameter (α) are considered ($\alpha = 0$ and 0.5). A simple comparison between

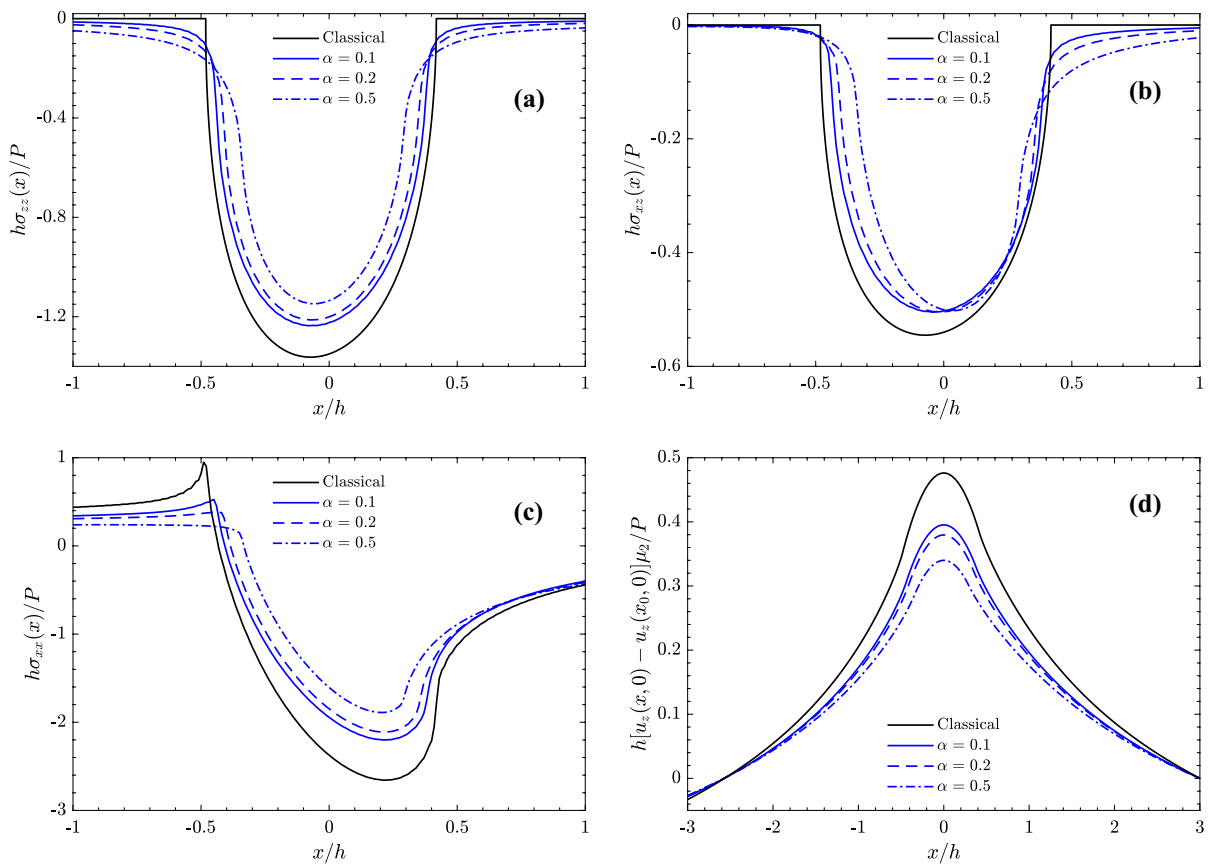


Fig. 16 The effects of the dimensionless parameter α on (a) normal stress σ_{zz} , (b) shear stress σ_{xz} , (c) tangential stress σ_{xx} , and (d) subsidence displacement u_z ($\eta = 0.4, \Gamma = 1/3$)

the two subfigures shows that the peak value of the subsidence displacement takes place under the rigid cylinder and decreases apparently with the inclusion of surface effects. For both cases, the subsidence displacement decays monotonically along the depth dimension of the graded layer.

6 Conclusions

We have successfully analyzed the sliding frictional nanocontact problem between a rigid cylinder and a graded layer perfectly bonded to a homogeneous half-plane. The sliding contact interface of the layer/substrate structure is modeled by Steigmann–Ogden surface mechanical theory. The

asymmetric contact pressure, contact boundaries, stresses and displacements are semianalytically evaluated. For the plane-strain nanocontact problem, Fourier integral transforms were employed to convert the governing equations and nonclassical mixed boundary conditions into a Fredholm integral equation. Together with the static force equilibrium equation, the integral equation was discretized and collocated with Gaussian quadratures, leading to an algebraic system with respect to discretized contact pressures and two asymmetric contact boundaries. Since the algebraic system is nonlinear about contact boundaries, an iterative algorithm was further developed. Compared with literature results, we additionally evaluated the full elastic fields along both the contact interface and

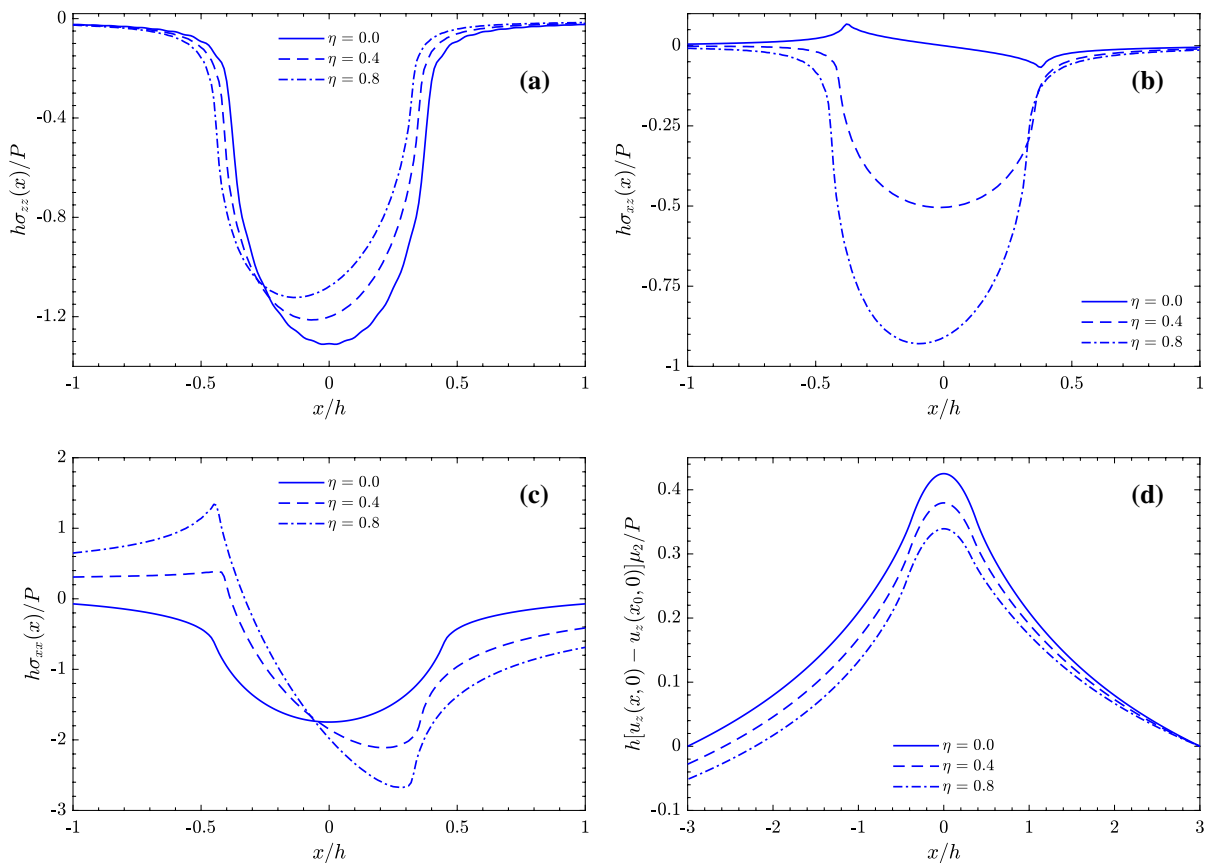


Fig. 17 The effects of sliding frictional coefficient η on **a** normal stress σ_{zz} , **b** shear stress σ_{xz} , **c** tangential stress σ_{xx} , and **d** subsidence displacement u_z ($\alpha = 0.2$, $\Gamma = 1/3$)

the depth dimension of the graded layer. A few important conclusions can be summarized from the extensive parametric studies about surface properties, sliding frictional coefficient and shear modulus gradation.

- Among the three Steigmann–Ogden surface parameters, the effects of surface tension are more significant than those of surface flexural rigidity. While both of them are important, the impact of surface membrane stiffness is marginal.
- When compared with classical solutions, higher contact pressures and smaller contact zones are found in nonclassical solutions with surface effects. Moreo-

ver, the pressures at both contact boundaries become nonzero. The sharp transitions of stresses across contact boundaries become more smooth.

- With increased sliding frictional coefficient, the contact zone deviates toward the frictional direction. The contact pressure on the sliding advancing side becomes appreciably larger than that of the receding side. While shear and tangential stresses increase with the frictional coefficients, an opposite trend is found for the normal stress and the subsidence displacement.
- Softer graded layers lead to higher subsidence displacements, lower peak contact pressures, and larger contact zones. The same argument remains valid for displacements and stresses.

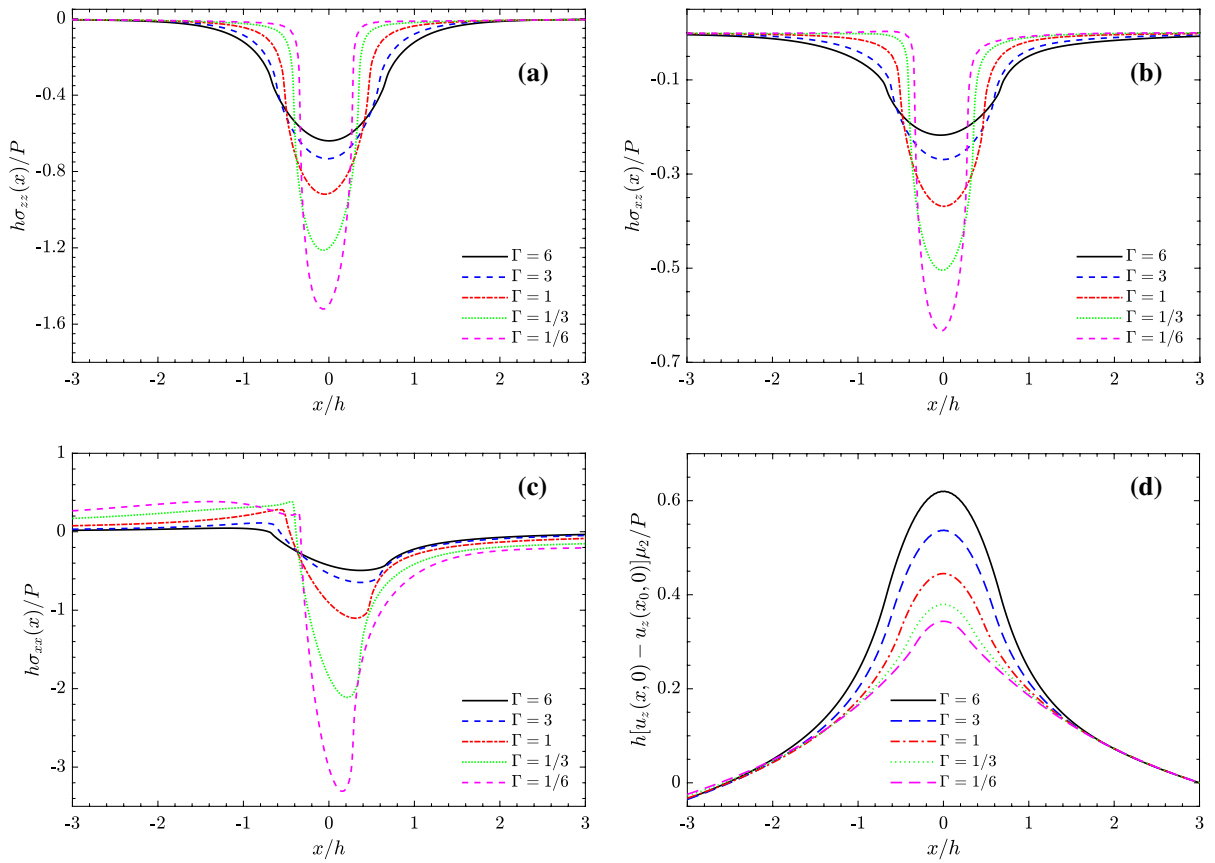


Fig. 18 The effects of shear moduli ratio Γ on **a** normal stress σ_{zz} , **b** shear stress σ_{xz} , **c** tangential stress σ_{xx} , and **d** subsidence displacement u_z ($\alpha = 0.2, \eta = 0.4$)

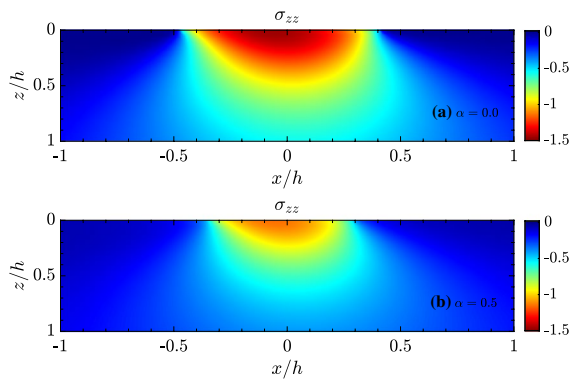


Fig. 19 Contour plots of the vertical stress σ_{zz} for (a) the classical and (b) the nonclassical cases inside a hard graded layer ($\eta = 0.4, \Gamma = 1/3$)

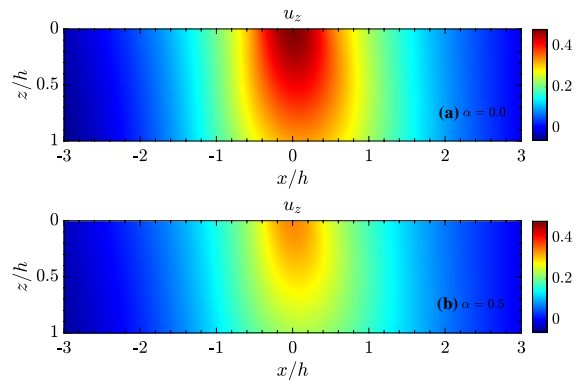


Fig. 20 Contour plots of the subsidence displacement u_z for (a) the classical and (b) the nonclassical cases inside a hard graded layer ($\eta = 0.4, \Gamma = 1/3$)

Although the full surface effects were considered in the sliding nanoindentation of a graded coating-substrate structure, the nanocontact behavior is characterized by the simple Column’s law of friction. In rolling and fretting contact problems, the whole contact zone is typically composed of a stick and a slip zone. This could be a natural extension of the current work. In the meanwhile, more efforts are also worth being made toward the coupling of microstructure and surface energy induced scale-dependency of small-scale graded materials and structures (Fathabadi and Alinia 2020).

Acknowledgements We gratefully acknowledge the support from the National Natural Science Foundation of China [grant numbers 12072072 & 11872149] and the Fundamental Research Funds for the Central Universities [grant number 2242022k30062].

Data availability The additional data that support the findings of this study are available from the corresponding author upon reasonable request.

Declarations

Conflict of interest The authors declare that they have no known conflict of interest.

Appendix A

The determinant M appearing in (7a, 7b) is defined by the coefficient matrix of the linear system

$$\begin{pmatrix} \Delta_1 & \Delta_2 & \Delta_3 & \Delta_4 & 0 & 0 \\ \Pi_1 & \Pi_2 & \Pi_3 & \Pi_4 & 0 & 0 \\ K_1 & K_2 & K_3 & K_4 & -2\mu_2 I \xi \cdot e^{-|\xi|h} & -2\mu_2 I \left(\frac{(1+\kappa)\xi}{2|\xi|} + \xi h \right) \cdot e^{-|\xi|h} \\ \Lambda_1 & \Lambda_2 & \Lambda_3 & \Lambda_4 & 2\mu_2 |\xi| \cdot e^{-|\xi|h} & -2\mu_2 \left(\frac{1-\kappa}{2} - |\xi|h \right) \cdot e^{-|\xi|h} \\ e^{m_1 h} & e^{m_2 h} & e^{m_3 h} & e^{m_4 h} & -e^{-|\xi|h} & -he^{-|\xi|h} \\ s_1 e^{m_1 h} & s_2 e^{m_2 h} & s_3 e^{m_3 h} & s_4 e^{m_4 h} & I \frac{\xi}{|\xi|} \cdot e^{-|\xi|h} & I \left(\frac{\xi}{|\xi|} h + \frac{\kappa}{\xi} \right) \cdot e^{-|\xi|h} \end{pmatrix} \begin{pmatrix} B_1 \\ B_2 \\ B_3 \\ B_4 \\ A_5 \\ A_6 \end{pmatrix} = \begin{pmatrix} -\tilde{q} \\ -\tilde{p} \\ 0 \\ 0 \\ 0 \\ 0 \end{pmatrix}, \tag{38}$$

where

$$\Delta_j = \mu_1 q_j - k_0 \xi^2, \tag{39}$$

$$\Pi_j = \frac{\mu_1}{\kappa - 1} p_j - (\tau_0 \xi^2 + d_0 \xi^4) s_j, \tag{40}$$

$$K_j = \mu_1 \frac{e^{(\beta+m_j)h}}{\kappa - 1} p_j, \tag{41}$$

$$\Lambda_j = \mu_1 e^{(\beta+m_j)h} q_j, \tag{42}$$

with $j = 1 - 4$ and

$$q_j = m_j - I \xi s_j, \tag{43}$$

$$p_j = -I \xi (3 - \kappa) + (1 + \kappa) m_j s_j. \tag{44}$$

References

Alinia, Y., Guler, M.A., Adibnazari, S.: On the contact mechanics of a rolling cylinder on a graded coating. Part 1: Analytical formulation. *Mech. Mater.* **68**, 207–216 (2014). <https://doi.org/10.1016/j.mechmat.2013.08.010>

Argatov, I.I., Chai, Y.S.: Optimal design of the functional grading in elastic wear-resisting bearings: a simple analytical model. *Int. J. Mech. Mater. Des.* **18**, 353–364 (2022). <https://doi.org/10.1007/s10999-021-09581-7>

Argatov, I.I., Sabina, F.J.: Spherical indentation of a transversely isotropic elastic half-space reinforced with a thin layer. *Int. J. Eng. Sci.* **50**, 132–143 (2012). <https://doi.org/10.1016/j.ijengsci.2011.08.009>

Arslan, O.: Plane contact problem between a rigid punch and a bidirectional functionally graded medium. *Eur. J. Mech. A-Solids* **80**, 103925 (2020). <https://doi.org/10.1016/j.euromechsol.2019.103925>

Arslan, O., Dag, S.: Contact mechanics problem between an orthotropic graded coating and a rigid punch of an arbitrary profile. *Int. J. Mech. Sci.* **135**, 541–554 (2018). <https://doi.org/10.1016/j.ijmecsci.2017.12.017>

Attia, M.A., El-Shafei, A.G.: Modeling and analysis of the nonlinear indentation problems of functionally graded elastic layered solids. *Proc. Inst. Mech. Eng. Part J-J. Eng. Tribol.* **233**, 1903–1920 (2019). <https://doi.org/10.1177/1350650119851691>

Attia, M.A., Mahmoud, F.F.: Analysis of nanoindentation of functionally graded layered bodies with surface elasticity. *Int. J. Mech. Sci.* **94–95**, 36–48 (2015). <https://doi.org/10.1016/j.ijmecsci.2015.02.016>

- Balci, M.N., Dag, S.: Solution of the dynamic frictional contact problem between a functionally graded coating and a moving cylindrical punch. *Int. J. Solids Struct.* **161**, 267–281 (2019). <https://doi.org/10.1016/j.ijsolstr.2018.11.020>
- Balci, M.N., Dag, S.: Moving contact problems involving a rigid punch and a functionally graded coating. *Appl. Math. Model.* **81**, 855–886 (2020). <https://doi.org/10.1016/j.apm.2020.01.004>
- Ban, Y., Mi, C.: On spherical nanoinhomogeneity embedded in a half-space analyzed with Steigmann-Ogden surface and interface models. *Int. J. Solids Struct.* **216**, 123–135 (2021). <https://doi.org/10.1016/j.ijsolstr.2020.11.034>
- Ban, Y., Mi, C.: On the competition between adhesive and surface effects in the nanocontact properties of an exponentially graded coating. *Appl. Math. Comput.* **432**, 127364 (2022). <https://doi.org/10.1016/j.amc.2022.127364>
- Cammarata, R.C.: Surface and interface stress effects in thin-films. *Prog. Surf. Sci.* **46**, 1–38 (1994). [https://doi.org/10.1016/0079-6816\(94\)90005-1](https://doi.org/10.1016/0079-6816(94)90005-1)
- Chen, P., Chen, S., Peng, J.: Sliding contact between a cylindrical punch and a graded half-plane with an arbitrary gradient direction. *J. Appl. Mech.-Trans. ASME* **82**, 041008 (2015). <https://doi.org/10.1115/1.4029781>
- Chen, S.H., Yao, Y.: Elastic theory of nanomaterials based on surface-energy density. *J. Appl. Mech.-Trans. ASME* **81**, 121002 (2014). <https://doi.org/10.1115/1.4029781>
- Chhapadia, P., Mohammadi, P., Sharma, P.: Curvature-dependent surface energy and implications for nanostructures. *J. Mech. Phys. Solids* **59**, 2103–2115 (2011). <https://doi.org/10.1016/j.jmps.2011.06.007>
- Choi, H.J., Paulino, G.H.: Thermoelastic contact mechanics for a flat punch sliding over a graded coating/substrate system with frictional heat generation. *J. Mech. Phys. Solids* **56**, 1673–1692 (2008). <https://doi.org/10.1016/j.jmps.2007.07.011>
- Comez, I., Erdol, R.: Frictional contact problem of a rigid stamp and an elastic layer bonded to a homogeneous substrate. *Arch. Appl. Mech.* **83**, 15–24 (2013). <https://doi.org/10.1007/s00419-012-0626-4>
- Dag, S., Guler, M.A., Yildirim, B., Ozatag, A.C.: Frictional Hertzian contact between a laterally graded elastic medium and a rigid circular stamp. *Acta Mech.* **224**, 1773–1789 (2013). <https://doi.org/10.1007/s00707-013-0844-z>
- Elloumi, R., Kallel-Kamoun, I., El-Borgi, S.: A fully coupled partial slip contact problem in a graded half-plane. *Mech. Mater.* **42**, 417–428 (2010). <https://doi.org/10.1016/j.mechmat.2010.01.002>
- Erdogan, F., Gupta, G.D.: Numerical solution of singular integral-equations. *Q. Appl. Math.* **29**, 525–534 (1972). <https://doi.org/10.1090/qam/408277>
- Erdogan, F., Gupta, G. D., Cook, T.S.: Numerical solution of singular integral equations. In: Sih, G.C. (Ed.), *Methods of Analysis and Solutions of Crack Problems: Recent Developments in Fracture Mechanics - Theory and Methods of Solving Crack Problems* (pp. 368–425). (1973). Springer Netherlands, Dordrecht. https://doi.org/10.1007/978-94-017-2260-5_7
- Fathabadi, S.A.A., Alinia, Y.: A nano-scale frictional contact problem incorporating the size dependency and the surface effects. *Appl. Math. Model.* **83**, 107–121 (2020). <https://doi.org/10.1016/j.apm.2020.02.017>
- Gad, A.I., Mahmoud, F.F., Alshorbagy, A.E., Ali-Eldin, S.S.: Finite element modeling for elastic nano-indentation problems incorporating surface energy effect. *Int. J. Mech. Sci.* **84**, 158–170 (2014). <https://doi.org/10.1016/j.ijmecsci.2014.04.021>
- Giannakopoulos, A.E., Suresh, S.: Indentation of solids with gradients in elastic properties: Part I. Point force. *Int. J. Solids Struct.* **34**, 2357–2392 (1997). [https://doi.org/10.1016/S0020-7683\(96\)00171-0](https://doi.org/10.1016/S0020-7683(96)00171-0)
- Gradshteyn, I.S., Ryzhik, I.M.: *Table of Integrals, Series, and Products* (8th). Elsevier Academic Press, Boston (2015)
- Guler, M.A., Erdogan, F.: Contact mechanics of graded coatings. *Int. J. Solids Struct.* **41**, 3865–3889 (2004). <https://doi.org/10.1016/j.ijsolstr.2004.02.025>
- Guler, M.A., Erdogan, F.: The frictional sliding contact problems of rigid parabolic and cylindrical stamps on graded coatings. *Int. J. Mech. Sci.* **49**, 161–182 (2007). <https://doi.org/10.1016/j.ijmecsci.2006.08.006>
- Guler, M.A., Kucuksucu, A., Yilmaz, K.B., Yildirim, B.: On the analytical and finite element solution of plane contact problem of a rigid cylindrical punch sliding over a functionally graded orthotropic medium. *Int. J. Mech. Sci.* **120**, 12–29 (2017). <https://doi.org/10.1016/j.ijmecsci.2016.11.004>
- Gurtin, M.E., Murdoch, A.I.: Continuum theory of elastic-material surfaces. *Arch. Ration. Mech. Anal.* **57**, 291–323 (1975). <https://doi.org/10.1007/bf00261375>
- Gurtin, M.E., Murdoch, A.I.: Surface stress in solids. *Int. J. Solids Struct.* **14**, 431–440 (1978). [https://doi.org/10.1016/0020-7683\(78\)90008-2](https://doi.org/10.1016/0020-7683(78)90008-2)
- Intarit, P., Senjuntichai, T., Rungamornrat, J., Limkatanyu, S.: Influence of frictional contact on indentation of elastic layer under surface energy effects. *Mech. Res. Commun.* **110**, 103622 (2020). <https://doi.org/10.1016/j.mechrescom.2020.103622>
- Jobin, K.J., Abhilash, M.N., Murthy, H.: A simplified analysis of 2D sliding frictional contact between rigid indenters and FGM coated substrates. *Tribol. Int.* **108**, 174–185 (2017). <https://doi.org/10.1016/j.triboint.2016.09.021>
- Kucuksucu, A., Guler, M.A., Avci, A.: Mechanics of sliding frictional contact for a graded orthotropic half-plane. *Acta Mech.* **226**, 3333–3374 (2015). <https://doi.org/10.1007/s00707-015-1374-7>
- Le, T.M., Lawongkerd, J., Bui, T.Q., Limkatanyu, S., Rungamornrat, J.: Elastic response of surface-loaded half plane with influence of surface and couple stresses. *Appl. Math. Model.* **91**, 892–912 (2021). <https://doi.org/10.1016/j.apm.2020.09.034>
- Le, T.M., Wongviboonsin, W., Lawongkerd, J., Bui, T.Q., Rungamornrat, J.: Influence of surface and couple stresses on response of elastic substrate under tilted flat indenter. *Appl. Math. Model.* **104**, 644–665 (2022). <https://doi.org/10.1016/j.apm.2021.12.013>
- Li, X., Mi, C.: Effects of surface tension and Steigmann-Ogden surface elasticity on Hertzian contact properties. *Int. J.*

- Eng. Sci. **145**, 103165 (2019). <https://doi.org/10.1016/j.jengsci.2019.103165>
- Li, X., Mi, C.: Nanoindentation hardness of a Steigmann-Ogden surface bounding an elastic half-space. *Math. Mech. Solids* **24**, 2754–2766 (2019). <https://doi.org/10.1177/1081286518799795>
- Li, X., Mi, C.: Nanoindentation of a half-space due to a rigid cylindrical roller based on Steigmann-Ogden surface mechanical model. *Int. J. Mech. Mater. Des.* **17**, 25–40 (2021). <https://doi.org/10.1007/s10999-020-09507-9>
- Long, J.M., Wang, G.F.: Effects of surface tension on axisymmetric Hertzian contact problem. *Mech. Mater.* **56**, 65–70 (2013). <https://doi.org/10.1016/j.mechmat.2012.09.003>
- Long, J.M., Wang, G.F., Feng, X.Q., Yu, S.W.: Two-dimensional Hertzian contact problem with surface tension. *Int. J. Solids Struct.* **49**, 1588–1594 (2012). <https://doi.org/10.1016/j.ijsolstr.2012.03.017>
- Mi, C.: Surface mechanics induced stress disturbances in an elastic half-space subjected to tangential surface loads. *Eur. J. Mech. A-Solids* **65**, 59–69 (2017). <https://doi.org/10.1016/j.euromechsol.2017.03.006>
- Mi, C.: Elastic behavior of a half-space with a Steigmann-Ogden boundary under nanoscale frictionless patch loads. *Int. J. Eng. Sci.* **129**, 129–144 (2018). <https://doi.org/10.1016/j.jengsci.2018.04.009>
- Mi, C., Jun, S., Kouris, D.A., Kim, S.Y.: Atomistic calculations of interface elastic properties in noncoherent metallic bilayers. *Phys. Rev. B* **77**, 075425 (2008). <https://doi.org/10.1103/PhysRevB.77.075425>
- Moradweysi, P., Ansari, R., Gholami, R., Bazdid-Vahdati, M., Rouhi, H.: Half-space contact problem considering strain gradient and surface effects: An analytical approach. *Zeitschrift für Angewandte Mathematik und Mechanik* **99**, e201700190 (2019). <https://doi.org/10.1002/zamm.20170190>
- Pinyochotiwong, Y., Rungamornrat, J., Senjuntichai, T.: Rigid frictionless indentation on elastic half space with influence of surface stresses. *Int. J. Eng. Sci.* **71**, 15–35 (2013). <https://doi.org/10.1016/j.jengsci.2013.04.005>
- Rahman, A.A.A., El-Shafei, A.G., Mahmoud, F.F.: Influence of surface energy on the nanoindentation response of elastically-layered viscoelastic materials. *Int. J. Mech. Mater. Des.* **12**, 193–209 (2016). <https://doi.org/10.1007/s10999-015-9301-6>
- Schulz, U., Peters, M., Bach, F.W., Tegeeder, G.: Graded coatings for thermal, wear and corrosion barriers. *Mater. Sci. Eng. A-Struct. Mater. Proper. Microstruct. Process.* **362**, 61–80 (2003). [https://doi.org/10.1016/S0921-5093\(03\)00579-3](https://doi.org/10.1016/S0921-5093(03)00579-3)
- Shen, J.J.: Axisymmetric Boussinesq problem of a transversely isotropic half space with surface effects. *Math. Mech. Solids* **24**, 1425–1437 (2019). <https://doi.org/10.1177/1081286518797387>
- Shenoy, V.B.: Size-dependent rigidities of nanosized torsional elements. *Int. J. Solids Struct.* **39**, 4039–4052 (2002). [https://doi.org/10.1016/S0020-7683\(02\)00261-5](https://doi.org/10.1016/S0020-7683(02)00261-5)
- Steigmann, D.J., Ogden, R.W.: Plane deformations of elastic solids with intrinsic boundary elasticity. *Proc. Royal Soc. A-Math. Phys. Eng. Sci.* **453**, 853–877 (1997). <https://doi.org/10.1098/rspa.1997.0047>
- Steigmann, D.J., Ogden, R.W.: Elastic surface-substrate interactions. *Proc. Royal Soc. A-Math. Phys. Eng. Sci.* **455**, 437–474 (1999). <https://doi.org/10.1098/rspa.1999.0320>
- Suresh, S.: Graded materials for resistance to contact deformation and damage. *Science* **292**, 2447–2451 (2001). <https://doi.org/10.1126/science.1059716>
- Tirapat, S., Senjuntichai, T., Rungainornrat, J., Rajapakse, R.K.N.D.: Indentation of a nanolayer on a substrate by a rigid cylinder in adhesive contact. *Acta Mech.* **231**, 3235–3246 (2020). <https://doi.org/10.1007/s00707-020-02703-w>
- Vasu, T.S., Bhandakkar, T.K.: A study of the contact of an elastic layer-substrate system indented by a long rigid cylinder incorporating surface effects. *J. Appl. Mech.* **83**, 061009 (2016). <https://doi.org/10.1115/1.4033079>
- Vasu, T.S., Bhandakkar, T.K.: Plane strain cylindrical indentation of functionally graded half-plane with exponentially varying shear modulus in the presence of residual surface tension. *Int. J. Mech. Sci.* **135**, 158–167 (2018). <https://doi.org/10.1016/j.ijmecsci.2017.11.009>
- Walton, J.R., Zemlyanova, A.Y.: A rigid stamp indentation into a semiplane with a curvature-dependent surface tension on the boundary. *SIAM J. Appl. Math.* **76**, 618–640 (2016). <https://doi.org/10.1137/15M1044096>
- Wang, L.: Boussinesq problem with the surface effect based on surface energy density. *Int. J. Mech. Mater. Des.* **16**, 633–645 (2019). <https://doi.org/10.1007/s10999-019-09476-8>
- Yan, J., Mi, C.: On the receding contact between an inhomogeneously coated elastic layer and a homogeneous half-plane. *Mech. Mater.* **112**, 18–27 (2017). <https://doi.org/10.1016/j.mechmat.2017.05.007>
- Yang, J., Ke, L.-L.: Two-dimensional contact problem for a coating-graded layer-substrate structure under a rigid cylindrical punch. *Int. J. Mech. Sci.* **50**, 985–994 (2008). <https://doi.org/10.1016/j.ijmecsci.2008.03.002>
- Zemlyanova, A.Y.: Frictionless contact of a rigid stamp with a semi-plane in the presence of surface elasticity in the Steigmann-Ogden form. *Math. Mech. Solids* **23**, 1140–1155 (2018). <https://doi.org/10.1177/1081286517710691>
- Zemlyanova, A.Y.: An adhesive contact problem for a semi-plane with a surface elasticity in the Steigmann-Ogden form. *J. Elast.* **136**, 103–121 (2019). <https://doi.org/10.1007/s10659-018-9694-1>
- Zemlyanova, A.Y., Mogilevskaya, S.G.: Circular inhomogeneity with Steigmann-Ogden interface: Local fields, neutrality, and Maxwell's type approximation formula. *Int. J. Solids Struct.* **135**, 85–98 (2018). <https://doi.org/10.1016/j.ijsolstr.2017.11.012>
- Zhang, G.P., Sun, K.H., Zhang, B., Gong, J., Sun, C., Wang, Z.G.: Tensile and fatigue strength of ultrathin copper films. *Mater. Sci. Eng. A-Struct. Mater. Proper. Microstruct. Process.* **483–84**, 387–390 (2008). <https://doi.org/10.1016/j.msea.2007.02.132>
- Zhang, X., Wang, Q.J., Wang, Y., Wang, Z., Shen, H., Liu, J.: Contact involving a functionally graded elastic thin film and considering surface effects. *Int. J. Solids Struct.* **150**, 184–196 (2018). <https://doi.org/10.1016/j.ijsolstr.2018.06.016>
- Zhao, X.J., Rajapakse, R.K.N.D.: Analytical solutions for a surface-loaded isotropic elastic layer with surface energy

- effects. *Int. J. Eng. Sci.* **47**, 1433–1444 (2009). <https://doi.org/10.1016/j.ijengsci.2008.12.013>
- Zhao, X.J., Rajapakse, R.K.N.D.: Elastic field of a nano-film subjected to tangential surface load: Asymmetric problem. *Eur. J. Mech. A-Solids* **39**, 69–75 (2013). <https://doi.org/10.1016/j.euromechsol.2012.11.005>
- Zhou, S., Gao, X.L.: Solutions of half-space and half-plane contact problems based on surface elasticity. *Z. Angew. Math. Phys.* **64**, 145–166 (2013). <https://doi.org/10.1007/s00033-012-0205-0>
- Zhou, Y., Lin, Q., Yang, X., Hong, J., Zhang, N., Zhao, F.: Material stiffness optimization for contact stress distribution in frictional elastic contact problems with multiple load cases. *Int. J. Mech. Mater. Des.* **17**, 503–519 (2021). <https://doi.org/10.1007/s10999-021-09544-y>
- Zhu, X., Zhai, J.-H., Xu, W.: Analysis of surface-loaded problem of nonhomogeneous elastic half-plane with surface tension. *Mech. Mater.* **129**, 254–264 (2019). <https://doi.org/10.1016/j.mechmat.2018.11.008>

Publisher's Note Springer Nature remains neutral with regard to jurisdictional claims in published maps and institutional affiliations.

Springer Nature or its licensor (e.g. a society or other partner) holds exclusive rights to this article under a publishing agreement with the author(s) or other rightsholder(s); author self-archiving of the accepted manuscript version of this article is solely governed by the terms of such publishing agreement and applicable law.